Topsoil-foraging root system architecture and N-use efficiency governed by small-effect QTL coevolved during jute (Corchorus olitorius L.) domestication

Pratik Satya
Nur Alam Mandal
Biswanath Adhikary
Avrajit Chakraborty
Debajeet Das
Avijit Kundu
Jiban Mitra
Dipnarayan Saha
Subhojit Datta
Ajay Kumar Mahato
Sabyasachi Mitra
Amit Bera
Chandan Sourav Kar
Kishor Gaikwad
Gouranga Kar
Ramcharan Bhattacharya
Debabrata Sarkar
Nagendra Kumar Singh
nksingh4@gmail.com

ICAR - National Institute for Plant Biotechnology https://orcid.org/0000-0002-7753-8517

Research Article

Keywords: Corchorus olitorius, Crop domestication, Gene network, Nitrate reductase, QTL mapping, Root system architecture, Single nucleotide polymorphism

Posted Date: August 20th, 2025

DOI: https://doi.org/10.21203/rs.3.rs-7263845/v1

Abstract

Background and Aims

The genetic basis of topsoil-foraging root system architecture (RSA) contrary to a steep-cheap-deep root ideotype typical of most annual crops and how it has evolved in jute (*Corchorus olitorius*) during its domestication as a bast-fibre crop are unknown.

Methods

For jute is cross-incompatible with wild *Corchorus* species, we used a population (F_2-$F_{2:3}$) founded by a *bast fibre-shy* mutant with impaired fibre development, nitrate reductase activity (NRA) and RSA and its corresponding wild-type (WT). To detect QTL for leaf and root NRA, 11 RSA-related traits and shoot biomass, we generated whole-plant transcriptomes and constructed a genome-integrated genetic map comprising both genic and genomic SNPs.

Results

We identified a total of 154 QTL anchoring 107 unique SNP loci, with 140 exerting small effects. However, 75 % of these QTL were identified as multi-trait QTL associated with 42 SNP loci suggesting a well-coordinated pleiotropic genetic control of NRA and RSA. By analyzing and relating the mutant to WT ratios of the QTL number, additive effects and explained phenotypic variance over the 14 traits, we showed that additive effects contributed to tweaking the RSA. We identified many QTL with regulatory roles and reconstructed a multidimensional QTL gene network of the complex interactions governing the RSA in jute characterized by much lower root to shoot ratio (RSR).

Conclusion

A gradual domestication of topsoil-foraging RSA in jute was driven by the coordinated actions of many small-effect QTL, with an interplay of above- and below-ground NRA modulated by key regulatory genes stabilizing its RSR.

Introduction

The fundamental challenge a plant faces is to optimize and allocate resources to both above- and below-ground biomass (Boonman et al. 2020). Most dicot annual crops are thus characterized by a penetrating deep taproot system that offers a better opportunity for nutrient and water uptake. In fact, a steep-cheap-deep (SCD) root ideotype accounts for better soil resource acquisition in crops (Lynch 2022). In contrast, natural vegetation adopts a topsoil-foraging shallow-root ideotype as the resources like water, nutrient and oxygen progressively decline while soil resistance intensifies with an increasing soil depth (van der Bom et al. 2020). The efficacy of the root system in fostering the above-ground biomass is often measured by two indicators—root to shoot biomass ratio (RSR) and the maximum rooting depth to plant/canopy height ratio (D_R: H_S). Although both these indicators widely fluctuate depending on species and

environmental conditions, most of the plants except for those with fibrous root systems adopt an SCD ideotype, with D_R: H_S and RSR close to 1.0 (Tumber-Dávila et al. 2022) and 0.5 (Ledo et al. 2018), respectively. There are many examples where plants invest more in root biomass, particularly under nutrient-deficient and resource-limiting conditions (Boonman et al. 2020, Hodge 2009, Lopez et al. 2023). Whereas a converse root ideotype with low D_R: H_S and RSR is rare among crop plants. Since the most limiting nutrients like organic carbon, nitrogen (N), extractible phosphorus (P) and exchangeable potassium (K) have the shallowest distribution with plant-cycling being the dominant form of nutrient recycling (Jobbágy and Jackson 2001), a denser root system in the topsoil would be advantageous for rapid transport of nutrient to the above-ground biomass. Hence, an in-depth understanding of the root system architectures (RSA) of shallow-rooted crops that foster high above-ground biomass could be useful for developing an energy-efficient topsoil-foraging root ideotype uncharacteristic of most annual crops.

Jute (*Corchorus olitorius* L., Malvaceae, 2n = 2*x* = 14), a secondary-phloic bast-fibre crop, is an outstanding example of a shallow-rooted crop that fosters high above-ground biomass (20–25 t ha^{-1} DW) within 3–4 months under a long-day (LD) photoperiod (Satya and Maiti 2013), which may perhaps be the highest amongst the annual crops (Satya et al. 2022b). The unbranched jute stem reaches a height over 3 m above the ground, while the primary taproot penetrates only up to 40 cm below the ground, with a D_R: H_S and an RSR of 0.13 (Changdee et al. 2008) and 0.3 (Fawusi and Ormrod 1981), respectively. Most interestingly, with such a remarkably low D_R: H_S ratio, jute root system affords about 5–10 times heavier vertically-erect above-ground biomass (Dhar et al. 2018). By comparison, taproots of most of the high biomass-producing dicots penetrate even up to 1.5 m below the ground (Fan et al. 2016). Moreover, the RSR of jute is also lower than that of most of the trees (0.5; Ledo et al. 2018) suggesting that its soil-resource uptake efficiency and root anchorage as manifested by roots' architectural distribution within a small surface area are quite unique among the crop plants.

Of the major nutrients, N is the most limiting factor for biomass accumulation and crop yield (Marschner 2011). The nitrate (NO_3^-) being the main N source for plants is predominantly available in the top 20–30 cm of the soil (Jobbágy and Jackson 2001, Russi et al. 2024). Even in the deep-rooted crops like maize, the highest N and P uptakes occur within a soil depth of 30 cm (Perkins and Lynch 2021). Hence, it is logical to hypothesize that a shallow-rooted plant that accumulates high above-ground biomass would have a typical RSA for maximizing the NO_3^- assimilation. Nitrate reductase (NR) is the first enzyme in the NO_3^- assimilation pathway catalyzing the reduction of NO_3^- to nitrite (NO_2^-). Recent evidence suggests that NR is involved in root-architecture remodeling via auxin- and nitric oxide-mediated pathways (Correa-Aragunde et al. 2016). It is, therefore, worth investigating whether the development of jute's unique topsoil-foraging RSA is associated with the NR activity.

Apropos this unique biology of jute, the genetic basis of its RSA is still poorly understood. Our current understanding of the genetics of its root traits is based on a handful of combining-ability studies on traits like lateral root length and number, root angle and biomass and taproot length, suggesting a

significant role of dominance variance for most of these traits (Basak 1993). Constrained by a narrow genetic base, however, these diallel-cross studies reported contradictory results giving a rather long rigamarole that could hardly elucidate the genetic basis of the complexity and uniqueness of the root system in jute. Mapping quantitative trait loci (QTL) is a robust approach for dissecting the genetic basis of the complex root traits and deciding chromosomal locations of unknown genes. However, till date only one root QTL, that too for root weight, has been reported in *C. olitorius* (Kundu et al. 2015). Low genetic diversity limiting the scope for the identification of suitable founders (of mapping populations), an inherent difficulty in phenotyping the root traits in the field (Richards 2008, Paez-Garcia et al. 2015), experimental errors associated with phenotyping the RSA using mature field-grown plants (Bai et al. 2013, Liu et al. 2013, Kundu et al. 2015) and low genetic polymorphism together with high segregation distortion (Mir et al. 2008, 2009, Das et al. 2012, Topdar et al. 2013, Kundu et al. 2015, Yang et al. 2019) were the key issues resulting in the dearth of information on the inheritance vis-à-vis genetics of root traits in jute. Earlier, we developed a RAD-SNP genetic map of jute from a bi-parental population for QTL mapping of bast-fibre yield and yield components (Kundu et al. 2015). Enriching this map with new SNP markers would obviously aid in improving the precision of QTL mapping. Of obvious note, genic-SNPs are particularly useful for QTL mapping of agronomic traits since they are associated with the coding regions (Zhao et al. 2019). Yet, genetic map as such is not particularly useful for the identification of genes underlying the QTL unless they are linked to genomic information. Hence, the integration of the genetic map with the genome sequence can lead to precise location of novel genomic regions associated with QTL and understanding the interactions of those QTL for various target traits at the genetic level (Govindarajulu et al. 2021).

For the uniqueness of RSA involving functional coordination of several root traits, we hypothesized here that the highly efficient topsoil-foraging root system in jute might have coevolved in association with N-use efficiency (NUE) during the process of its domestication as a bast-fibre crop. Hence, the genes controlling these traits are most likely to have a high probability of being colocalized on the jute genome at specific chromosomal regions. To aptly attest and validate our hypothesis, we detected QTL for NR activity (NRA) and RSA, identified their genomic locations and examined their functional relationships by i) discovering, validating and mapping genic SNPs, ii) constructing a genome-integrated genetic map comprising both genic and genomic SNPs, iii) phenotyping the seedling root traits under a hydroponic system aided by digital image-capture and analyses, iv) mapping QTL based on multiple-QTL model (MQM), v) analyzing the underlying roles of small-effect QTL, and vi) reconstructing the resulting QTL gene network (QGN). Our study goes in some way, without claiming any expressive originality, toward revalidating Jack Rodney Harlan's Neo-Darwinian theory (Harlan 1975) of crop domestication.

Materials and methods

Plant material

C. olitorius cv. JRO-632, a popular high-yielding cultivar and Sudan Green (SG, accession no. OEX-031), an African *C. olitorius* landrace extensively utilized in jute breeding program, were used in the present

study for RNA-Seq. They were collected from the National Active Germplasm Site for Jute and Allied Fibres (ICAR-Central Research Institute for Jute and Allied Fibres, Barrackpore, Kolkata), and were selfed for one generation to ensure genetic purity. Harvested seeds were grown in a controlled environment chamber (28°C Day/ 25°C night temperature, 80% RH and a 16-h photoperiod of 35 Wm^{-2}) for 7 days. Leaf, root and stem tissues from a pool of 50 plants were flash-frozen in liquid N_2 and stored at -86°C; also, fresh, non-dormant seeds were powdered with LN_2. The SG (♀) × *bast fibre-shy* (*bfs*) mutant (♂) F_2 population, as reported earlier (Kundu et al. 2015), was used for Illumina GoldenGate® genotyping. Its 168 $F_{2:3}$ families were phenotyped under hydroponics for root traits because the mutant in addition to its characteristic ribbon leaves (a recessive trait with a 3:1 F_2 segregation ratio) and defective bast-fibre development also had an impaired root system compared to its wild-type (WT) SG (Kundu et al. 2012).

Transcriptome sequencing by RNA-Seq

Total RNA was extracted using Invitrogen's (Thermo Fisher Scientific Inc., Waltham) high-quality RNA isolation protocol using TRIzol® with PureLink™ RNA Mini Kit, according to manufacturer's instruction. RNA purity and integrity were checked by Agilent's RNA 6000 Pico Kit on Agilent 2100 Bioanalyzer (Agilent Technologies Inc., Santa Clara). Equal volumes of RNA from each tissue (leaf, root, seed and stem) were mixed to constitute the RNA pool for each genotype. The pooled RNA representing the whole-plant transcriptomes of JRO-632 and SG were sequenced on a Roche 454 GS FLX platform (Roche Holding AG, Basel). Sequencing libraries were prepared using Roche 454 GS-FLX kits, according to GS FLX Titanium Series October 2009 (Rev. Jan 2010). The cDNA library quality was checked using high-sensitivity DNA chip on Agilent 2100 Bioanalyzer. The libraries were amplified by emulsion-based PCR and deposited on pico-titer plate for pyrosequencing on Roche 454 GS FLX. Since combining different assemblers offers more credible result for 454 reads (Kumar and Blaxter 2010), the transcriptomes were assembled de novo using the cDNA assembly features of GS De novo Assembler, CLC Genomics Workbench, SeqMan Ngen and CAP3. The assembled transcriptomes were aligned against several databases (NCBI Nr, SwissProt, KEGG and COG) using BLASTx (*E*-value < 10^{-5}) to extract the protein coding sequences (CDS) and gene annotations. The Nr-annotated database was mapped to gene ontology (GO) database (Ashburner et al. 2000) as implemented in OmicsBox (Conesa et al. 2005). Aligned unigenes were mapped to the KEGG database using KAAS (KEGG Automatic Annotation Server; Moriya et al. 2007).

Genic-SNP discovery and validation

High-quality Roche GS FLX reads of the two transcriptomes were assembled with MiRA 4.0 (Chevreux et al. 2004) and mapped with GSMapper (Roche Holding AG, Basel) with a seed length of 16, minimum overlap length of 70 and minimum overlap identity of 95. The SNPs on terminal regions and with < 75 bp flanking regions were discarded. Also, SNPs from InDels, low complexity regions and intron/ exon splice junctions were filtered out. A subset of SNPs (> 2000) were validated by PCR (initial denaturation at 95°C for 5 minutes followed by 35 cycles of denaturation at 95°C for 30 s, annealing at a temperature specific for each primer pair for 30 s and primer extension at 72°C for 45 s) followed by resolving in 1.5% agarose

gel (110 v, 30 min). Robust SNPs showing distinct polymorphism were further validated by Sanger sequencing using big-dye terminator v3.1 chemistry on Genetic Analyzer 3730xl (Thermo Fisher Scientific Inc., Waltham). Amplicons that generated good sequences were further manually curated and subjected to bioinformatic SNP validation using CLC Genomics Workbench. The SNPs with high mapping quality and design score were retained for further downstream analyses.

Illumina GoldenGate® OPA and genotyping

We used Illumina (Illumina Inc., San Diego) GoldenGate® custom oligonucleotide pooled assay (OPA: GS0014193-OPA; test version: 09464019) containing both allele- and locus-specific oligos to design a panel of 384 SNPs. The final SNP selection was based on i) heterozygosity of the target SNP in founder genotypes, ii) the absence of additional polymorphisms adjacent to the target SNP, iii) SNPs located within 50 bp to sequence ends or intron/ exon splice junctions and iv) the absence of polymorphism in mapped sequence reads. A > 0.6 designability-rank score was selected to obtain a high success rate for the conversion of SNPs into a successful GoldenGate® OPA as suggested by Hyten et al. (2008). The 'GoldenGate® Genotyping Assay for VeraCode Manual Protocol' (Illumina Inc., San Diego, USA) was performed using Illumina's BeadArray Express, according to the standard manufacturer's protocol as described earlier (Hyten et al. 2008, Gaur et al. 2015). Briefly, DNA was normalized to 50 ng μl^{-1} in 96-well plates, activated by adding 5 µl MS1 reagent to 250 ng (5 µl of 50 ng μl^{-1}) of DNA and incubated at 95°C for 30 min to prepare single-use DNA. DNA samples were hybridized to six GoldenGate GT UNIV32 bead Chips having 384 SNP-probes for 176 samples, and the fluorescence signal on the bead Chip was analyzed by iScan BeadArray Reader (Illumina Inc., San Diego).

Genome-integrated genetic map construction

We excluded genic-SNP markers with highly significant ($P \leq 0.001$) segregation distortions against the expected 1:2:1 F_2 segregation ratio and then constructed a functional genic-SNP-based genetic map using R/qtl (Broman et al. 2003), with an error probability of 0.01. This resulting SG × *bfs* genic-SNP genetic map was integrated with its corresponding genomic RAD-SNP genetic map reported earlier (Kundu et al. 2015). Finally, we used Chromonomer v1.07 (Catchen et al. 2020) to integrate the draft genome of *C. olitorius* cv. JRO-524 (Sarkar et al. 2017) into the integrated genetic map, with default settings, such as, re-scaffolding the contigs based on the genetic map and using a minimum of two markers to anchor a scaffold (or contig) on a particular map node.

Phenotyping seedling root traits under hydroponics

Seeds of 168 SG × *bfs* $F_{2:3}$ families and their two founders were surface-disinfested with 0.1% $HgCl_2$ and germinated in sterile Petri dishes (35 mm) on moist filter papers followed by culturing them on filter-paper wicks in 10-ml polycarbonate tubes containing ½-strength Hoagland's nutrient solution (pH 5.8). After 3 days, the nutrient solution was changed to full-strength and thereafter replenished every 2 days. The experiment was laid out in a completely randomized design (CRD), with six replications each with 3

seedlings, under a 16-h photoperiod (180 µmol m^{-2} s^{-1} light intensity) at 32 ^{o}C and 80% RH. After 14 days, plants were carefully harvested, kept in 30% alcohol, and their images were captured under dark using AlphaImager 3400 (Alpha Innotech, Kasendorf). The images were analyzed using DIRT v1.0 (Das et al. 2015), IJ_Rhizo (Pierret et al. 2013) and ImageJ (Schneider et al. 2012), with respective default settings. Following image capture, plants were oven-dried overnight at 70 ^{o}C. Data of 11 RSA-related traits, viz., average root density (RD), average root diameter (ARD, mm), equivalent root surface area (ERSA, mm^2), equivalent root volume (RV, mm^3), lateral root number (LRN), maximum root length (MRL, cm), projected root surface area (PRA, mm^2), root diameter at the base (RDB, mm), root tissue angle (RTA, °), root weight (RW, mg $plant^{-1}$) and total root length (TRL, mm) were collected. In addition, we also recorded the shoot weight (SW, mg $plant^{-1}$) representing the above-ground biomass. Nitrate reductase (NR) activities in leaf (LNRA, µmol h^{-1} g FW^{-1}) and root (RNRA, µmol h^{-1} g FW^{-1}) were estimated, according to Scheible et al. (1997) using Sigma (Sigma-Aldrich, St. Louis) chemicals and reagents.

QTL mapping

The QTL analyses were performed using the software MapQTL6 (build: 10oct2022.24feb2020, licence: 28011.1458; Kyazma B. V., Wageningen; Van Ooijen 2009). The genome-integrated SG × *bfs* genetic map comprising a total of 382 markers (317 genomic RAD-SNPs and 65 genic-SNPs) was used for QTL mapping using the mean data of each trait. For each trait, both chromosome- and genome-wide LOD significance thresholds ($P \leq 0.05$) for QTL peaks were determined using 10,000 permutations. Initially, non-parametric Kruskal-Wallis rank sum test (*d. f.* = 2) was performed to estimate genome-wide single marker influence. Finally, QTL were detected based on multiple-QTL model (MQM) employing automatic cofactor selection (ACS) with backward elimination at a minimum map distance of 2.0 cM followed by MQM mapping based on the regression model (Haley and Knott 1992) using the selected cofactors. This resulted in the fitting of a single segregating QTL in the background of cofactors, with genetic effects of separate QTL modelled as additive fixed effects. Though both definitive (genome-wide significant) and suggestive (chromosome-wide significant) QTL were detected, we reported here only the definitive ones, and their 2-LOD support intervals and graphs were drawn using MapChart 2.2 (Voorrips 2002). The confidence interval (CI) of the QTL location was calculated, according to Li (2011).

QTL network reconstruction

To identify the candidate genes underlying the QTL, we performed a blastn search of the SNP locus on or nearest to the QTL peak to the predicted and annotated genes of the draft genome of *C. olitorius* cv. JRO-524 (Singh and Sarkar 2022). Since there is little information on protein-protein association of *C. olitorius*, the network reconstruction using *C. olitorius* in the String database (Szklarczyk et al. 2023) resulted in a poor network structure. Hence, corresponding *Arabidopsis thaliana* protein homologs were identified from the String database and used as an input query in Genemania (Franz et al. 2018) to reconstruct the gene interaction network employing the automatically selected weighting method as suggested by Doroshkov et al. (2019). Finally, the network was trimmed retaining the QTL gene homologs and further processed in Cytoscape (Shannon et al. 2003).

Statistical analyses

The $F_{2:3}$ phenotypic data were first tested for heteroscedasticity using Bartlett's and Shapiro-Wilk tests ($P \leq 0.05$). Heteroscedastic data were accordingly log- (ERSA, LRN, PRA, RDB, RTA, RV, RW and TRL) and square root-transformed (ARD, MRL and RD) prior to computing one-way analyses of variance (ANOVAs) based on the model as suggested by Kearsey and Pooni (1996) for $F_{2:3}$ families. The additive genetic variance (V_A) and narrow-sense heritability (h^2) were calculated as $V_A = \sigma^2_B$ and $h^2 = V_A/(V_A + V_E)$, where σ^2_B and V_E ($\sigma^2_W - ½V_A$) represent variance between and environmental variance within families, respectively, while σ^2_W is the variance within families. The coefficient of additive genetic variation (CV_A) was calculated, according to Houle (1992). Pearson's product-moment correlations were used to test trait associations at a significance threshold of $P \leq 0.05$. The relationships between the ratios of the QTL number, additive effects (a) and explained phenotypic variance (r^2) over the 14 traits were worked out by fitting linear regressions. All statistical analyses were conducted in R version 4.1.3 (R Core Team 2022).

Results

NRA and RSA phenotypes of jute

Though the mutant had considerably lower RW (54%) and SW (55%) than that of its corresponding WT (Fig. 1a), there was no difference in RSR between the two (Fig. 1b). However, the mutant was characterized by an impaired root system (Fig. 1c, d) as evident by about 50% reduction in ERSA, LRN, MRL, PRA, RD, RV and TRL (Table 1). This might have resulted in weaker associations between the root traits in the mutant than in its WT (Fig. 1e). Though RW had significant ($P \leq 0.05$) positive correlations with ERSA, PRA, RV and TRL in the WT, it was not correlated with either of the root traits in the mutant. Both LNRA and RNRA were two-fold higher in the WT, with six- to seven-fold higher activity in the leaf than in the root. The SG × *bfs* $F_{2:3}$ families were characterized by substantial genetic variation for all the phenotypic traits (Table 1), but they were positively skewed toward the female founder (WT) for most of the traits except for RDB and RTA. Besides, most of the root traits had significant ($P \leq 0.05 - 0.001$) positive correlations between themselves. Despite a highly significant ($P \leq 0.001$) positive correlation ($r = 0.67$) between RW and SW, no significant ($P \leq 0.05$) correlations were observed between LNRA/ RNRA and root traits. The h^2 was intermediate ($0.25 \leq h^2 \leq 0.5$) for ARD, RDB and RTA, whereas it was > 0.5 for the other traits, varying from 0.6 for RV to even 1.0 for both LNRA and RNRA (Table 1). A high h^2 combined with high transgressive segregation indeed offered a better genetic background for the QTL mapping of RSA in the SG × *bfs* mapping population. The CV_A was the lowest for RDB (7.6%) and the highest for TRL (38.0%), while it was very high for both LNRA (77.0%) and RNRA (80.7%).

Table 1
Trait means for the two founders and $F_{2:3}$ families of the SG × *bfs* mapping population, with estimates of narrow-sense heritability (h^2) and coefficient of additive genetic variation (CV_A)

Trait[a]	Sudan Green	*bfs*	Mid-founder value	$F_{2:3}$			h^2	CV_A
				Mean (±)	Min	Max		
ARD (mm)	0.80 ± 0.04	0.66 ± 0.03	0.73	0.82 ± 0.005	0.45	2.18	0.490	12.16
ERSA (mm^2)	805.22 ± 81.00	364.10 ± 23.15	584.66	399.48 ± 5.31	177.66	1820.50	0.676	30.04
LNRA (µmol h^{-1} gFW^{-1})	4.730 ± 0.077	2.381 ± 0.051	3.556	2.563 ± 0.063	0.005	12.649	0.100	77.00
LRN	19.90 ± 1.59	11.70 ± 0.99	15.80	12.80 ± 0.16	4.00	47.00	0.556	25.69
MRL (cm)	3.84 ± 0.41	2.92 ± 0.19	3.38	2.63 ± 0.02	1.01	6.13	0.682	19.10
PRA (mm^2)	256.31 ± 25.78	115.90 ± 7.37	186.11	127.16 ± 1.69	56.55	579.48	0.676	30.03
RD	1.60 ± 0.12	1.10 ± 0.11	1.35	1.49 ± 0.01	0.33	3.79	0.307	16.12
RDB (mm)	8.26 ± 0.11	8.30 ± 0.35	8.28	7.92 ± 0.03	3.80	10.33	0.448	7.55
RNRA (µmol h^{-1} gFW^{-1})	0.749 ± 0.009	0.343 ± 0.017	0.546	1.238 ± 0.031	0.005	5.706	0.100	80.68
RTA (°)	63.36 ± 1.51	63.18 ± 5.01	63.27	57.87 ± 0.38	23.74	79.78	0.329	11.20
RV (mm^3)	144.44 ± 11.08	58.31 ± 4.67	101.38	77.43 ± 1.04	33.35	432.70	0.547	27.97
RW (mg $plant^{-1}$)	25.90 ± 2.25	11.92 ± 0.78	18.91	13.32 ± 0.17	6.10	48.80	0.755	30.09

[a] ARD, average root diameter; ERSA, equivalent root surface area; LNRA, leaf nitrate reductase activity; LRN, lateral root number; MRL, maximum root length; PRA, projected root surface area; RD, average root density; RDB, root diameter at the base; RNRA, root nitrate reductase activity; RTA, root tissue angle; RV, equivalent root volume; RW, root weight; SW, shoot weight; TRL, total root length

Trait[a]	Sudan Green	*bfs*	Mid-founder value	$F_{2:3}$			h^2	CV_A
SW (mg plant^{-1})	64.96 ± 3.65	29.32 ± 2.47	47.14	28.52 ± 0.31	7.90	89.30	0.852	26.57
TRL (mm)	366.54 ± 53.09	183.89 ± 13.26	275.22	169.22 ± 2.69	47.67	688.85	0.789	38.01

[a] ARD, average root diameter; ERSA, equivalent root surface area; LNRA, leaf nitrate reductase activity; LRN, lateral root number; MRL, maximum root length; PRA, projected root surface area; RD, average root density; RDB, root diameter at the base; RNRA, root nitrate reductase activity; RTA, root tissue angle; RV, equivalent root volume; RW, root weight; SW, shoot weight; TRL, total root length

A genome-integrated genetic map of jute

We obtained 800,093 and 820,169 high-quality clean 454 reads that were assembled into 31,484 (TSA: GFDO00000000.1) and 32,628 (TSA: GFDJ00000000.1) transcripts representing the whole-plant transcriptomes yielding 10,841 and 13,944 SNPs in *C. olitorius* cvs JRO-632 and SG, respectively, which upon filtration retained a set of 1,385 genic-SNPs. Of these, 1,068 were validated by Sanger sequencing followed by designing and synthesizing 2,136 primers that produced 1,208 clean amplicons in both JRO-524 and SG. By validating the 308 genic-SNPs in CLC Genomics Workbench and selecting another 76 based on mapping quality and design score, we designed a 384-SNP panel for Illumina GoldenGate® genotyping of the SG × *bfs* F_2 mapping population. The genic-SNP linkage map involving a total of 113 SNPs retrieved from 92 transcripts (Online Resource 1, Table S1) consisted of seven linkage groups (LGs), with an average marker interval and a total genetic length of 3.34 cM and 346.3 cM, respectively in close agreement with the RAD-SNP genetic map (358.5 cM) reported earlier using the same population (Kundu et al. 2015). The length of an individual LG varied from 13.2 cM (LG6) to 108.7 cM (LG2). This genic-SNP map upon integration with the genomic RAD-SNP map (Kundu et al. 2015) when further integrated with the draft genome sequence of *C. olitorius* cv. JRO-524 produced the first genome-integrated genetic map of jute consisting of 382 reference markers (317 genomic RAD-SNPs and 65 genic-SNPs) across seven LGs, with an average length and marker interval of 52 cM/1,404,439 bp and 1.2 cM/25,735.8 bp, respectively and a total genetic length of 365.7 cM (Fig. 2) in close agreement with that of either the genic-SNP or RAD-SNP map. LG2 was the longest (112.2 cM) and LG6 the shortest (13.2 cM), with maximum (104) and minimum (14) number of markers, respectively. A total of 239 mapped markers (178 RAD and 61 genic-SNPs) were assigned (*E*-value < $1e^{-15}$) to 206 genes as predicted and annotated in the JRO-524 draft genome, with LG1 and LG2 with 98 and 104 markers corresponding to 60 and 70 genes with known functions and gene ontologies, respectively.

QTL for NRA and RSA in jute

Altogether, we identified a total of 154 QTL for 14 traits corresponding to 107 unique SNP loci (88 genomic RAD-SNP and 19 genic-SNP loci) at a genome-wide (GW) LOD significance threshold of 3.5

(Fig. 3a; Online Resource 1, Table S2). Of these, 81 markers were on top of QTL peaks, while 26 were within the CI of the QTL location. The LOD score of each of these QTL was ≥ 3.5, with 89 supported by a LOD score of ≥ 5.0. The maximum number of QTL was detected on LG2 (54) followed by LG1 (33), whereas the minimum on LG5 (4). On LG1 and LG2, the QTL were distributed throughout with an average distance of 2.71 cM and 3.29 cM, respectively between the two consecutive QTL. However, on LG3 and LG5, the QTL crowded the peripheries, with an average distance of 3.98 and 5.68 cM, respectively. The QTL were distributed sparsely on LG5 (0.18/ cM) to more densely on LG4 (0.71/ cM). The maximum number of QTL was detected for RDB (19), LNRA, LRN and MRL (17 each), SW (16), RW (13) and RNRA (10) (Online Resource 1, Table S2). A total of 14 major QTL (r^2 > 10%) were detected in our study (Table 2), with the mutant founder contributing the additive effects to the four of them. Two major QTL each were identified for LNRA, MRL and RW, with *qMRL-I2-8* explaining the greatest proportion of phenotypic variance (19.9%). Notwithstanding this result, most of the QTL (140) identified for root traits in our study were polygenic explaining < 10% (small-effect) of phenotypic variance (r^2) but supported by rather high LOD scores well above the GW significance threshold (3.5) at $P \leq 0.05$.

Table 2
Major NRA and RSA QTL detected in the SG × *bfs* population of jute

Trait[a]	QTL	LG	LOD threshold[b]	Peak (cM)	LOD	Nearest marker[c]	*a*[d]	*d*[d]	r^2 (%)[e]
ARD	*qARD-l1-2*	1	3.5 (2.8)	32.4	7.0	**Co_Sb0324**	0.020	0.046	12.1
ERSA	*qERSA-l2-2*	2	3.6 (3.0)	97.9	6.4	**Co_Sb0441**	0.362	0.341	10.4
LNRA	*qLNRA-l3-3*	3	3.6 (2.8)	69.3	12.2	**Co_Sb0526**	-0.789	0.001	10.8
	qLNRA-l7	7	3.6 (2.2)	0.0	12.5	Co_1664 – 990	0.261	-0.261	11.1
LRN	*qLRN-l1-1*	1	3.5 (2.8)	1.7	10.1	**Co_Sb0335**	-0.239	-0.006	10.0
MRL	*qMRL-l2-8*	2	3.6 (3.0)	83.6	16.7	Co_Sb0306	0.088	-0.247	19.9
	qMRL-l5	5	3.6 (2.3)	22.7	10.0	Co_5584 – 813	-0.003	0.124	10.8
RNRA	*qRNRA-l1-4*	1	3.6 (2.8)	29.1	7.8	**Co_Sb0315**	-0.265	-0.216	10.7
RTA	*qRTA-l2-1*	2	3.6 (3.0)	18.1	7.3	Co_Sb0183	-0.094	-0.107	14.3
RV	*qRV-l2-2*	2	3.6 (3.0)	108.7	6.4	**Co_7810 – 1032**	0.166	-0.015	10.6
RW	*qRW-l1*	1	3.6 (2.8)	36.7	9.9	Co_Sb0307	0.064	-0.166	11.2
	qRW-l2-3	2	3.6 (3.0)	108.7	9.0	**Co_7810 – 1032**	0.170	0.011	10.0
SW	*qSW-l7-1*	7	3.6 (2.2)	19.1	10.0	**Co_Sb0572**	0.218	0.319	10.6

[a] As in Table 1

[b] Genome- and chromosome-wide (within parenthesis) LOD significance threshold values at $P \leq 0.05$ based on 10,000 permutations of the experimental data

[c] Markers suffixed with alphanumeric and numeric characters represent genomic and genic SNP loci, respectively, and those in boldface are associated with multi-trait QTL

[d] *a*, additive effect; *d*, dominance effect

[e] Phenotypic variance explained by a QTL as estimated at the highest probability peak

Trait[a]	QTL	LG	LOD threshold[b]	Peak (cM)	LOD	Nearest marker[c]	*a*[d]	*d*[d]	r^2 (%)[e]
TRL	*qTRL-l3-2*	3	3.6 (2.9)	59.1	7.8	**Co_Sb0506**	0.180	-0.267	12.5

[a] As in Table 1

[b] Genome- and chromosome-wide (within parenthesis) LOD significance threshold values at $P \leq 0.05$ based on 10,000 permutations of the experimental data

[c] Markers suffixed with alphanumeric and numeric characters represent genomic and genic SNP loci, respectively, and those in boldface are associated with multi-trait QTL

[d] *a*, additive effect; *d*, dominance effect

[e] Phenotypic variance explained by a QTL as estimated at the highest probability peak

The QTL additive effects were nearly equally contributed by the WT (81 QTL) and its mutant (73 QTL) (Online Resource 1, Table S2). We determined the mutant: WT ratios of the QTL number (QTL ratio), a trait's total additive effects (additive-effect ratio) and phenotypic variance explained by the QTL (r^2 ratio) for each trait and compared them with the corresponding mutant: WT phenotypic trait-value ratios (Fig. 3b). These ratios were in close agreement with most of the root traits except for ARD, ERSA, RD and RTA indicating reliable concordance of the founder phenotypes and the QTL effects for most of the root traits. A significant ($P = 0.008$) linear association between the additive-effect and r^2 ratios further implied that the additive effects contributed significantly to the QTL variance of the RSA. Moreover, a strong, positive linear association ($P \leq 0.001$) of QTL ratio with the additive-effect and r^2 ratios ($P \leq 0.001$) over the 14 traits posited the additive nature of QTL in both the mutant and its WT (Fig. 3c).

Genomic regions colocalizing the QTL for multiple root traits in jute

About 75% of the QTL (115) identified in our study were colocalized multi-trait QTL associated with 42 SNP loci (2–6 QTL/ SNP) suggesting a well-coordinated genetic control of the topsoil-foraging RSA in jute (Online Resource 1, Table S3). Of the 42 loci, 22, 12 and 6 anchored 2, 3 and 4 colocalized QTL, respectively. The loci *Co_4733 – 237* and *Co_Sb0608* were mapped on five and six QTL, respectively. Interestingly, nine out of the 14 major QTL were also identified as multi-trait QTL (Table 2). The colocalization of 90% RNRA QTL with the other root QTL evidenced for strong pleiotropic gene effects controlling NR synthesis in root tissues. Furthermore, all the ARD and ERSA, 88.2% LRN, 78.9% RDB, 77.8% RD and 76.5% LNRA QTL were multi-trait QTL. Of the 42 loci, 27 anchored colocalized QTL that received additive effects from only one founder (Fig. 4a), further confirming pleiotropic gene actions. Whereas a total of 15 loci were associated with QTL from both the founders. This might well substantiate a rather high degree of transgressive segregation as recorded in the SG × *bfs* population. A more precise relationship between QTL and r^2 ratios ($R^2 = 0.95$, $P \leq 0.001$) was obtained (Fig. 4b) based

on only multi-trait QTL (115) than on all the QTL (154) identified (Fig. 3c). Besides RNRA, we identified RD as a key trait governed by more QTL contributed by the mutant explaining a greater proportion of phenotypic variance. To note, eight LNRA, six RNRA and five RD QTL contributed by the mutant explained 41.5, 43.3 and 33.2% of phenotypic variance (r^2), respectively (Fig. 4a).

Candidate genes for NRA and RSA in jute

Of the 107 physically mapped SNPs, 68 were annotated (*E*-value < $1e^{-10}$) to 81 protein-coding genes, which were classified as 194 and 65 distinct GO identities and terms, respectively (Online Resource 1, Table S4). This enabled us to identify corresponding protein-coding genes associated with 32 SNP loci anchoring 89 multi-trait QTL (Table 3). The locus *Co_Sb0608* anchoring the maximum number of QTL (6) was found to code for a microtubule-binding protein involved in cytoskeletal organization being associated with six GO identities. Whereas the locus *Co_4733 – 237* anchoring five QTL corresponded to a gene for 'SCF ubiquitin ligase complex', which is involved in protein degradation in many signal transduction pathways. The locus *Co_Sb0052* associated with the maximum number of GO identities (17) was mapped to a gene coding for the master immune regulator 'NPR1' (see below). Similarly, the locus *Co_Sb0335* coding for 'DNA polymerase epsilon catalytic subunit A-like isoform X1' was associated with 15 GO identities indicating its general role in root development in jute. Since many annotated multi-trait QTL (19) were anchored to the LNRA and RNRA loci, NR could be assumed to play a pivotal role in determining the RSA in jute. The proteins annotated for these QTL were involved in diverse GO pathways including 'SCF ubiquitin ligase complex protein', 'MALE DISCOVERER 2-like isoform X1', 'NPR1', 'lysine-specific demethylase ELF6', 'beta-adaptin-like protein A', 'two-component response regulator-like PRR37', 'protein phosphatase 2C 75' and 'abscisic acid receptor PYL4-like' (Table 3; Online Resource 1, Table S4).

Table 3
Genes associated with multi-trait QTL for NRA and RSA detected in the SG × *bfs* population of jute

SNP locus[a]	Trait[b]	Gene[c]	Protein
Co_1392 – 521	LNRA, LRN, PRA	*LLWS01000016.1.g140*	26S proteasome non-ATPase regulatory subunit 11 homolog
Co_2487 – 988	LNRA, RNRA, SW	*LLWS01000720.1.g122*	Probable apyrase 6
Co_2521 – 1025	LNRA, RNRA, SW	*LLWS01001793.1.g2*	Protein IQ-DOMAIN 31
Co_2846 – 286	ARD, MRL	*LLWS01004155.1.g120*	Vacuolar protein 8-like
Co_4733 – 237	ARD, LNRA, MRL, RD, RDB	*LLWS01000264.1.g33*	SCF ubiquitin ligase complex protein
Co_513– 1455	LNRA, MRL	*LLWS01000506.1.g22*	MALE DISCOVERER 2-like isoform X1
Co_7810 – 1032	RDB, RV, RW	*LLWS01004386.1.g94*	Magnesium transporter MRS2-1
Co_99–693	RD, RDB	*LLWS01000127.1.g38*	Chlorophyll a-b binding protein CP29.1
Co_Sb0027	ARD, MRL, RD	*LLWS01000197.1.g12*	Putative glucuronosyltransferase PGSIP8
Co_Sb0052	RNRA, TRL	*LLWS01000253.1.g69*	NPR1
Co_Sb0059	RDB, RV, RW, SW	*LLWS01000304.1.g75*	Protein TSSC4
Co_Sb0072	PRA, TRL	*LLWS01000981.1.g78*	Acyl-CoA synthetase family member 4
Co_Sb0111	LNRA, LRN	*LLWS01001699.1.g8*	Soluble secretory phospholipase A2 receptor
Co_Sb0178	LRN, RDB	*LLWS01000013.1.g100*	Histone deacetylase complex subunit SAP18-like
Co_Sb0189	ERSA, LNRA	*LLWS01002255.1.g112*	Tetratricopeptide-like helical/ protein binding

[a] SNP locus associated with multi-trait QTL; loci suffixed with alphanumeric and numeric characters represent genomic and genic loci, respectively

[b] As in Table 1

[c] Genes predicted based on RNA-Seq evidence and annotated in the draft genome of *C. olitorius* cv. JRO-524

SNP locus[a]	Trait[b]	Gene[c]	Protein
Co_Sb0243	LNRA, LRN, RDB, SW	*LLWS01001136.1.g70*	Two-component response regulator-like PRR37 isoform X1
Co_Sb0252	LRN, RTA	*LLWS01000163.1.g114*	Signal recognition particle receptor subunit alpha-like
Co_Sb0264	MRL, RNRA	*LLWS01005408.1.g95*	Probable ADP-ribosylation factor GTPase-activating protein AGD14 isoform X2
Co_Sb0298	LNRA, LRN, RDB	*LLWS01007630.1.g45*	Abscisic acid receptor PYL4-like
Co_Sb0309	ARD, LRN, RDB	*LLWS01000205.1.g69*	Transketolase, chloroplastic
Co_Sb0310	ERSA, LRN, RNRA	*LLWS01013921.1.g31*	G-type lectin S-receptor-like serine/threonine-protein kinase RLK1
Co_Sb0335	LRN, RDB	*LLWS01001019.1.g16*	DNA polymerase epsilon catalytic subunit A-like isoform X1
Co_Sb0380	ERSA, RW	*LLWS01002938.1.g46*	Probable disease resistance protein At1g12280
		LLWS01014603.1.g118	Probable disease resistance protein At5g63020
		LLWS01013700.1.g42	Putative disease resistance protein family
		LLWS01010483.1.g34	Cc-NBS-LRR resistance protein, putative
Co_Sb0404	RD, SW	*LLWS01002798.1.g84*	DNA-directed RNA polymerase 1B
Co_Sb0441	ERSA, PRA, TRL	*LLWS01000080.1.g122*	Putative LRR receptor-like serine/threonine-protein kinase
Co_Sb0442	ARD, RDB, SW	*LLWS01001397.1.g117*	Cation/calcium exchanger 1
Co_Sb0460	LRN, RNRA	*LLWS01000135.1.g135*	Probable protein phosphatase 2C 75
Co_Sb0482	LNRA, LRN, MRL, RDB	*LLWS01004543.1.g9*	21 kDa protein-like

[a] SNP locus associated with multi-trait QTL; loci suffixed with alphanumeric and numeric characters represent genomic and genic loci, respectively

[b] As in Table 1

[c] Genes predicted based on RNA-Seq evidence and annotated in the draft genome of *C. olitorius* cv. JRO-524

SNP locus[a]	Trait[b]	Gene[c]	Protein
Co_Sb0506	LRN, PRA, RW, TRL	*LLWS01006268.1.g1*	Zinc finger, U1-type
Co_Sb0526	LNRA, SW	*LLWS01010438.1.g91*	ABSCISIC ACID-INSENSITIVE 5-like protein 7
Co_Sb0572	RD, SW	*LLWS01002829.1.g52*	Homeobox-leucine zipper protein HDG2-like isoform X1
Co_Sb0608	LNRA, LRN, MRL, RDB, RNRA, RW	*LLWS01000113.1.g39*	65-kDa microtubule-associated protein 3-like isoform X1cytokinesis by cell plate formation

[a] SNP locus associated with multi-trait QTL; loci suffixed with alphanumeric and numeric characters represent genomic and genic loci, respectively

[b] As in Table 1

[c] Genes predicted based on RNA-Seq evidence and annotated in the draft genome of *C. olitorius* cv. JRO-524

Reconstruction of a QTL gene network (QGN) in jute

We validated all the 81 protein-coding genes associated with the root QTL by identifying corresponding homologs in other species including the model plant *Arabidopsis thaliana*, thereby suggesting that the genes controlling RSA are well conserved across plant families (Online Resource 1, Table S5). Our QGN was primarily based on the co-expression database Gene Expression Omnibus (87.2%) followed by shared protein domain (9.1%). The initial network comprising 84 nodes (genes) retained 63 homologs of root QTL-associated genes, providing strong evidence for functional coordination of RSA in jute. The loci *Co_4733 – 237* (ARD, LNRA, MRL, RD and RDB) and *Co_5277 – 157* (LNRA) were among the top five nodes as assessed by the degree value, betweenness centrality of the nodes, radiality and stress. A reduced representation of the network entailing 61 nodes represented the functional QGN of RSA in jute (Fig. 4c).

Discussion

Seedling root traits are a proxy for mature root system in jute

Since seedling RSA is an indicator of the growth and functioning of the mature root system later in the season (Løes and Gahoonia 2004), controlled experiments were widely employed to detect QTL for seedling roots traits (Tuberosa et al. 2002, Bai et al. 2013, Liu et al. 2017). Albeit, inconsistent correlations between seedling and mature root traits were reported in wheat, a monocot (Rich et al. 2020). By comparison to monocots, dicots, however, develop the main structures (tap root and basal roots with their respective laterals) of the root system at the seedling stage, and the mature root system is considered just an extension of those structures (Zhao et al. 2017). In jute (a dicot), plant height (PH)

and stem-base diameter (SBD) are the two most important target traits for improving fibre yield (FY) because fibre and seeds cannot be harvested from the same plant (Basak 1993, Satya et al. 2022b). The coincidence of several NRA and RSA QTL detected here with those for PH, FY, RW and SBD as reported earlier (Kundu et al. 2015) using field-grown mature plants (see Online Resource 1, Table S6) allowed us not only to identify the genomic regions (and genes) controlling these correlated traits, but to validate our current QTL results based on seedling root traits. Incidentally, the lone root-weight QTL (*qRW-l1*) reported earlier across multi-environments using the mature 120-day-old root system (Kundu et al. 2015) was also detected in the present study (*qRW-l1*) on LG1 corresponding to the same set of RAD-SNP loci defined by a 2-LOD score drop. Furthermore, the RAD-SNP locus *Co_Sb0608* on LG2 anchoring the multi-trait QTL for LNRA, LRN, MRL, RDB, RNRA and RW (Online Resource 1, Table S3) was also reported to be associated with the QTL for PH and SBD (Online Resource 1, Table S6). Given that bast fibre production was an important artificial selection pressure (Sarkar et al. 2019), the colocalization of these QTL can be construed as an above-ground selection-drag resulting in unconscious selection of the below-ground root traits including RNRA during jute domestication (see below). Taken together, we could thus unambiguously validate the usefulness of seedling root traits as a proxy for mature root system in jute.

QTL mapping suggests gradual domestication of RSA in jute

Though QTL mapping was extensively used to elucidate the domestication of key agronomic traits in major crop plants (Paterson 2002, Pan et al. 2017), only a few of those explored as to how RSA could have played a role in that process (Chen et al. 2022). Whereas an interspecific mapping population could well be an obvious choice for the identification of domestication-related QTL, the existence of a strong sexual-incompatibility barrier between the cultivated and wild jute consistently failed to produce viable progenies over the past several decades, and even when the progenies were somehow rescued, they heavily skewed to the female founder in F_2 onwards (Swaminathan and Iyer 1961, Kumar et al. 2022). This is not unexpected because even the cultivated jute was characterized by rather high segregation distortion (see Introduction), with most of the distorted loci being biased toward the female founder (Topdar et al. 2013, Kundu et al. 2015, this study). Moreover, sparsely fibrous wild *Corchorus* species, as opposed to their two cultivated fibre-type adelphotaxa, were reported to have deeper root systems with a high RSR (Choudhary et al. 2017). Against the backdrop of this evolutionary quagmire, the origin and evolution of the cultivated jute with its unique shallow and topsoil-foraging RSA that fosters high above-ground biomass is simply enigmatic and indeed stays a mystery. It has long been argued that a few QTL with large phenotypic effects were mainly implicated in domestication of the key above-ground traits in crop plants, whereas the small-effect QTL that stand for a typical signature of gradual evolution played a minor role in that process (Paterson 2002, Ross-Ibarra 2005). Whether the same is true for the below-ground traits, which were unconsciously selected during crop domestication, is an open question.

Our QTL mapping using a population with a mutant, with impaired root and shoot developments (Kundu et al. 2012, 2015) as one of the founders, allowed us to examine the relation between the above-ground conscious selection for profuse vegetative growth that induces bast-fibre development under a LD photoperiod (Sarkar et al. 2016) and below-ground unconscious selection for the root traits. Our results

underpinned that the genetic control of the RSA in jute was primarily determined by small-effect QTL in agreement with the Neo-Darwinian theory of crop domestication (Harlan 1975). That 91% of the QTL mapped in our study had small effects would unequivocally evidence for a gradual domestication of root traits in jute. Despite developing a high-density genome-integrated genetic map comprising both genic and genomic SNPs retrieved from high-quality whole-plant transcriptomes and a population characterized by rather high transgressive segregation, we could only identify 14 major QTL (Table 2). In parallel with our results, many small-effect QTL for above-ground traits like anatomical fibre content (FC), FY, PH and SBD as well as a below-ground trait like RW were earlier detected in the same mapping population (Kundu et al. 2015). In addition, most of the QTL identified for seed germination under salt stress in *C. olitorius* (Yang et al. 2019) and that for PH in *C. capsularis* (Tao et al. 2017) were also reported to exert small effects.

Although the small-effect QTL were traditionally ignored in search for large-effect QTL that could be deployed in molecular breeding (Moose and Mumm 2008), these QTL had convincingly been shown to be implicated in domestication and plant-architecture determination in a number of crop plants (Wills and Burke 2007, Wang et al. 2018, Wang et al. 2022). Hence, the prevalence of small-effect QTL for not only the root traits but the above-ground traits like SW and LNRA as identified in our study—in close agreement with all earlier reports (Das et al. 2012, Topdar et al. 2013, Kundu et al. 2015, Tao et al. 2017, Yang et al. 2019)—might well reinforce their crucial role in designing the jute plant architecture through gradual domestication. A significant positive association between the QTL number and their total additive effects offered a rather tenable support for the additive genetic control of the RSA in jute. Interestingly, the QTL additive effects were positively associated with the phenotypic variance explained by them (contributed by both the mutant and the WT founders). Being a predominantly inbred crop (Satya et al. 2014), dominance is, however, not expected to be a major determining factor for jute domestication (Moyers et al. 2018). For the mutant founder contributed additive effects to all the root traits under study, the phenotypic expressions of the root traits are expected to be coordinated. That 75% of the QTL corresponded to colocalized QTL for different traits with the same QTL peaks also implied a pleiotropic gene action of these small-effect QTL. The colocalization of QTL for multiple above-ground traits like fibre fineness, FY, PH was earlier reported in jute (Das et al. 2012, Topdar et al. 2013, Kundu et al. 2015). Incidentally, the fact that the annotated molecular functions of these loci were diverse could unambiguously rule out the occurrence of a few mutational changes. Several small-effect QTL were also found to be the major genetic determinant of root length and thickness in rice (Zhao et al. 2018). Of late, the genetic mechanism of RSA in soybean was also reported to be governed by small-effect QTL (Wang et al. 2022). The seminal root angle in bread wheat was also found to be under complex genetic control involving multiple small-effect QTL (Richard et al. 2018). The small-effect QTL governing the root anatomical traits in maize (Chen et al. 2022) further strengthened our hypothesis that these types of QTL might be the major driving force for gradual evolution of root traits. Unlike the domestication of above-ground traits driven primarily by the large-effect QTL, gradual changes brought about by many small-effect QTL account for the major genetic mechanism that might have driven unconscious domestication of below-ground RSA.

Root system's domestication is associated with NRA in jute

To substantiate our hypothesis that NRA coevolved with topsoil-foraging RSA in jute, we compared the phenotypic and QTL effects of the mutant versus the WT founders in terms of the QTL number, additive-effect and r^2 ratios (see Results). Firstly, we showed that the shallower RSA in the mutant founder resulted in a weaker association of root traits with an impaired NR activity. Phenotypic analyses of the mapping population revealed a high CV_A for LNRA and RNRA, whereas that for the other root traits were considerably low. For CV_A is an indicator of evolvability and traits closely associated with fitness are usually characterized by high CV_A (Garcia-Gonzalez et al. 2012), NRA could undoubtedly be assumed to be the key trait driving the evolution and domestication of jute. Secondly, the mutant founder contributing to the additive effects of 41.5 and 43.3% of LNRA and RNRA QTL, respectively could well corroborate its 50% reduction in NRA as compared to that in the WT founder. Thirdly, a ~ 1.5:1 ratio of the additive effects and r^2 of the RNRA QTL contributed by the mutant and the WT founders was in close agreement with the ratio of the number of QTL (1.5:1) contributed by them. Fourthly, 76.5 and 90% of the QTL governing LNRA and RNRA, respectively were mapped to the multi-trait QTL, with a greater proportion of the mutant for RNRA and the WT for LNRA. Finally, our network analysis revealed that many of the annotated loci associated with the NRA QTL represented regulatory proteins of diverse functions, with a strong connectivity with the root traits in our reconstructed QGN. Of note, the locus *Co_Sb0608* anchoring the highest number of QTL (6) explained large variations for LRN (7.5%), MRL (8.6%) and RNRA (8.5%). Incidentally, this locus codes for a 65-kDa microtubule-associated protein (MAP65) involved in cell division and cytokinesis. The Arabidopsis mutants for this locus (AtMAP65) had defective root and shoot morphogenesis via the formation of multinucleate, stubbed and gapped cell walls (Smertenko et al. 2004). Similarly, a mutation in the rice homolog OsMAP65 was reported to cause destabilization of phragmoplast formation in root apical meristem resulting in growth arrest (Lin et al. 2022). Since *Co_Sb0608* is not linked to the other QTL in our QGN, we have every reason to suggest that it may not be a component of the general root gene expression network common to plants characterized by a high RSR. Rather, it was observed to be linked with cellulose synthase. Since jute extensively synthesizes cellulosic fibre in the stem and also to a lesser extent in the root (Satya et al. 2022a) and bast fibre provides mechanical support to the plant (Meshram and Palit 2013), it is not unlikely that this locus might have specifically been selected during domestication of the fibre-type jute ecotypes to compensate for the weakening of mechanical support on account of a low RSR.

An interplay of above- and below-ground NRAs stabilizes the RSR in jute

In contrast to the SCD ideotype of maize, its wild progenitor teosinte, which is adapted to a nutrient-deficient condition, adopts a topsoil-foraging RSA developed by profuse lateral root branching and enhanced N-transport capacity (Schmidt et al. 2016). This clearly presupposes a linkage between N-uptake efficiency and lateral root development in shallow-rooted crops. As compared to the SCD crops where primary and lateral roots penetrate to a deeper level under drought stress, the rooting depth of jute grown in Africa was found to be < 25 cm under an optimum condition and declined further under water-

stressed conditions (Mgolozeli et al. 2022). Of obvious note, fibre-type jute ecotypes tend to develop more lateral roots under drought stress (Basak and Choudhuri 1967). In our study, a total of 15 (88%) LRN QTL were anchored to multi-trait QTL, of which 9 were from the WT founder. Besides, nine LRN QTL were also colocalized with four RNRA and five LNRA QTL in addition to those of other root traits. A gradual domestication of teosinte was concomitant with an unconscious selection of the below-ground biomass developing shorter and more branched nodal roots with higher root density while conserving the RSR for over 9000 years (Schmidt et al. 2016). Whereas its conscious selection of the above-ground biomass (tillering) was accompanied by an activation of *teosinte branched 1* (*tb1*), a repressor of lateral branch outgrowth by contributing to apical dominance (Flint-Garcia 2013). Thus, the domestication of topsoil-foraging RSA in jute, originated first in dry and harsh climate of Africa (Kundu et al. 2013) followed by its domestication as a bast-fibre crop with its typical tall unbranched ideotype, in the peninsular India (Sarkar et al. 2019) could well be dependent on an interplay of QTL governing the above- and below-ground NR syntheses modulating the lateral root number and root density and surface area while suppressing the above-ground lateral branch outgrowth. Our identification of a *Co_4733-237*-mapped gene that codes for SCF ubiquitin ligase (SCF^{TIR1}) as a hub gene of the root QGN (see below) lends a strong support to this hypothesis because SCF^{TIR1} is known to maintain apical dominance and promote lateral root development (Gray et al. 2003). The additive effects of four (*qARD-l2-1*, *qMRL-l2-1, qRD-l2-1* and *qRDB-l2-1*) out of the five QTL colocalized on *Co_4733 – 237* were contributed by the mutant parent, while the additive effect for *qLNRA-l2-1* was contributed by the WT parent. Interestingly, in accordance with the greater contribution of the WT founder to anchor LNRA as against RNRA QTL to the multi-trait QTL, the NRA was six-fold higher in the WT leaves than in its roots. Similarly, a ten-fold higher LNRA was reported in poplar implying its crucial role in the accumulation of biomass that fosters the growth of a tall, unbranched tree canopy (Black et al. 2002). By the way, signals transducing from root NR were also reported to play an important role in root growth and partitioning of the root-shoot biomass (Kruse et al. 2010). As evidenced by the anchored multi-trait QTL (see Results), it is thus quite plausible that a decreasing RNRA in the mutant resulted in lesser number of lateral roots concomitant with a decline in root density and surface area, thereby causing a weaker N-uptake efficiency vis-à-vis arresting its above-ground biomass growth.

A greater representation of LNRA or RNRA QTL in our QGN (Fig. 4b) could further reinforce the pivotal role of NRA in molding the RSA in jute. Since functional annotations identified many regulatory proteins involved in regulating the NRA (Table 3), we could clearly demonstrate that many of the QTL detected in our study have a regulatory role rather than directly being involved in metabolic pathways per se. For example, the gene mapped to the locus *Co_Sb0052* corresponding to the RNRA and TRL QTL codes for NPR1, which is a master regulator of salicylic acid (SA) controlling its interaction with other hormones besides interacting with both transcription activators as well as repressors (e.g., certain WRYKs; Zhou et al. 2023). In addition to its critical role in plant immunity, SA also plays an important role in plant growth and development. Phenylalanine, a precursor of SA, is ubiquitinated by SCF ubiquitin ligase to control SA biosynthesis (Spoel and Dong 2024). Indeed, the locus *Co_4733 – 237* colocalizing five QTL was annotated as SCF^{TIR1}. NR is also a potential source of NO that modulates TIR1 and genes involved in

lignin biosynthesis (Vitor et al. 2013). Since phenylalanine is also a key precursor of lignin biosynthesis pathway (Chakraborty et al. 2015) and the mutant is also defective in lignocellulosic bast-fibre production (Kundu et al. 2012), an increased pool of phenylalanine (in the mutant) may require fluxing more NR to NO conversion, thereby causing a deficiency of available NR to convert NO_3^- to NO_2^-. SCF^{TIR1} also modulates auxin-mediated root development, root hair growth and lateral root formation by activating auxin response factors (ARFs) through ubiquitination of Aux/IAA transcriptional repressors (Chen et al. 2025). In Arabidopsis, NO-mediated S-nitrosylation of cysteine residue of TIR1 enhances interaction of TIR1 and auxin (Aux/IAA) resulting in auxin degradation (Terrile et al. 2012). NR also modulates the root auxin balance to trigger new root formation and its elongation by activating the NO signaling pathway (Correa-Aragunde et al. 2016). Taken together, the colocalization of multiple QTL on *Co_4733 – 237*, a hub gene of our QGN, strongly suggests that TIR1 might have contributed to tweaking the RSA in jute by modulating root density, length and thickness. Whereas functional validation followed by biochemical assays would eventually define the NR-transduced major metabolic pathways in the future, our identification of QTL colocalizing the NR-regulatory genes strongly advocates their coordinated actions to stabilize the RSR in jute.

Declarations

Acknowledgments

We acknowledge Indian Council of Agricultural Research (ICAR)'s National Agriculture Science Fund (NASF) project GB-2018, ICAR-Network Project on Functional Genomics and Genetic Modifications (NPFGGM) sub-project ICAR-NPFGGM-3070, ICAR-Technology Mission on Jute (TMJ) project 18 – 17/TMJ/2013-14/378 and SERB-JC Bose National Fellowship (JCB/2022/000004) to NKS for funding. We also acknowledge the Xcelris Labs Ltd., Ahmedabad for assistance in Roche 454 GS-FLX sequencing and Illumina GoldenGate® OPA and genotyping.

Author contribution statement PS, DS, JM, SM and NKS conceived and planned the study; PS, NAM, BA, AC, DD, AK, JM, SM and AB phenotyped the population; DS, PS, AKM, NAM, AC, JM, DNS, SD, CSK and NKS generated the transcriptomes, and mined and validated the SNPs; PS, NAM, AC, AK, JM, DNS, SD, KG, RB, DS and NKS conducted the Illumina GoldenGateÒ OPA, genotyped the population and constructed the genetic maps; PS, BA, NAM, AC, DD, JM, CSK, GK, DS and NKS analyzed the data including QTL mapping; PS drafted the manuscript. All authors reviewed, edited and approved the final manuscript draft.

Conflict of interest The authors do not have any conflicts to declare.

Data availability The SRA and TSA sequences of Corchorus olitorius cv. JRO-632 (BioSample: SAMN06199045, SRA: SRR5145919, TSA: GFDO00000000.1) and C. olitorius cv. Sudan Green (BioSample: SAMN06199046, SRA: SRR5145920, TSA: GFDJ00000000.1) are publicly available at

DDBJ/EMBL/GenBank vide BioProject: PRJNA278717. The accessions of Sudan Green ´ *bfs* mapping population are available as BioSamples SAMN02838329 to SAMN02838506. The genotype data are deposited as a Figshare entry. https://doi.org/10.6084/m9.figshare.28877228

References

1. Ashburner M, Ball CA, Blake JA, Botstein D, Butler H, Cherry JM, Davis AP, Dolinski K, Dwight SS, Eppig JT, Harris MA, Hill DP, Issel-Tarver L, Kasarskis A, Lewis S, Matese JC, Richardson JE, Ringwald M, Rubin GM, Sherlock G (2000) Gene ontology: tool for the unification of biology. Nat Genet 25: 25-29. https://doi.org/10.1038/75556
2. Bai C, Liang Y, Hawkesford MJ (2013) Identification of QTLs associated with seedling root traits and their correlation with plant height in wheat. J Exp Bot 64: 1745-1753. https://doi.org/10.1093/jxb/ert041
3. Basak SL (1993) Quantitative genetics of fibre yield and its components. In: Denton IR (ed) Review on the genetics and breeding of jute. International Jute Organization, Dhaka, pp 51-95
4. Basak SL, Choudhuri BB (1967) Genetic variation and phenotypic plasticity of roots in two cultivated species of jute (*Corchorus olitorius* L. and *C. capsularis* L.). Biol Plant 9: 292-300. https://doi.org/10.1007/BF02929770
5. Black BL, Fuchigami LH, Coleman GD (2002) Partitioning of nitrate assimilation among leaves, stems and roots of poplar. Tree Physiol 22: 717-724. https://doi.org/10.1093/treephys/22.10.717
6. Boonman CCF, Langevelde Fv, Oliveras I, Couédon J, Luijken N, Martini D, Veenendaal EM (2020) On the importance of root traits in seedlings of tropical tree species. New Phytol 227: 156-167. https://doi.org/10.1111/nph.16370
7. Broman KW, Wu H, Sen S, Churchill GA (2003) R/qtl: QTL mapping in experimental crosses. Bioinformatics 19: 889-890. https://doi.org/10.1093/bioinformatics/btg112
8. Catchen J, Amores A, Bassham S (2020) Chromonomer: a tool set for repairing and enhancing assembled genomes through integration of genetic maps and conserved synteny. G3 10: 4115. https://doi.org/10.1534/g3.120.401485
9. Chakraborty A, Sarkar D, Satya P, Karmakar PG, Singh NK (2015) Pathways associated with lignin biosynthesis in lignomaniac jute fibres. Mol Genet Genom 290: 1523-1542. https://doi.org/10.1007/s00438-015-1013-y
10. Changdee T, Shigenori M, Jun A, Kaori I, Ryosuke T, and Polthanee A (2008) Root anatomical responses to waterlogging at seedling stage of three cordage fiber crops. Plant Prod Sci 11: 232-237. https://doi.org/10.1626/pps.11.232
11. Chen H, Qi L, Zou M, Lu M, Kwiatkowski M, Pei Y, Jaworski K, Friml J (2025) TIR1-produced cAMP as a second messenger in transcriptional auxin signalling. Nature 640: 1011-1016. https://doi.org/10.1038/s41586-025-08669-w

12. Chen Z, Sun J, Li D, Li P, He K, Ali F, Mi G, Chen F, Yuan L, Pan Q (2022) Plasticity of root anatomy during domestication of a maize-teosinte derived population. J Exp Bot 73: 139-153. https://doi.org/10.1093/jxb/erab406
13. Chevreux B, Pfisterer T, Drescher B, Driesel AJ, Müller WEG, Wetter T, Suhai S (2004) Using the miraEST assembler for reliable and automated mRNA transcript assembly and SNP detection in sequenced ESTs. Genome Res 14: 1147-1159. https://doi.org/10.1101/gr.1917404
14. Choudhary SB, Sharma HK, Anil Kumar A, Maruthi RT, Karmakar PG (2017) The genus *Corchorus* L. (Malvaceae) in India: species distribution and ethnobotany. Genet Resour Crop Evol 64: 1675-1686. https://doi.org/10.1007/s10722-016-0465-1
15. Conesa A, Götz S, García-Gómez JM, Terol J, Talón M, Robles M (2005) Blast2GO: a universal tool for annotation, visualization and analysis in functional genomics research. Bioinformatics 21: 3674-3676. https://doi.org/10.1093/bioinformatics/bti610
16. Correa-Aragunde N, Foresi N, Lamattina L (2016) Auxin and nitric oxide: a counterbalanced partnership ensures the redox cue control required for determining root growth pattern. Adv Bot Res 77: 41-54. https://doi.org/10.1016/bs.abr.2015.10.006
17. Das A, Schneider H, Burridge J, Ascanio AKM, Wojciechowski T, Topp CN, Lynch JP, Weitz JS, Bucksch A (2015) Digital imaging of root traits (DIRT): a high-throughput computing and collaboration platform for field-based root phenomics. Plant Methods 11: 51. https://doi.org/10.1186/s13007-015-0093-3
18. Das M, Banerjee S, Topdar N, Kundu A, Mir RR, Sarkar D, Sinha MK, Balyan HS, Gupta PK (2012) QTL identification for molecular breeding of fibre yield and fibre quality traits in jute. Euphytica 187: 175-189. https://doi.org/10.1007/s10681-011-0603-y
19. Dhar P, Ojha D, Kar CS, Mitra J (2018) Differential response of tossa jute (*Corchorus olitorius*) submitted to water deficit stress. Ind Crops Prod 112: 141-150. https://doi.org/10.1016/j.indcrop.2017.10.044
20. Doroshkov AV, Konstantinov DK, Afonnikov DA, Gunbin KV (2019) The evolution of gene regulatory networks controlling *Arabidopsis thaliana* L. trichome development. BMC Plant Biol 19: 53. https://doi.org/10.1186/s12870-019-1640-2
21. Fan J, McConkey B, Wang H, Janzen H (2016) Root distribution by depth for temperate agricultural crops. Field Crops Res 189: 68-74. https://doi.org/10.1016/j.fcr.2016.02.013
22. Fawusi MOA, Ormrod DP (1981) Photoperiod responses of *Corchorus olitorius* L. in controlled environments. Ann Bot 48: 635-638. https://doi.org/10.1093/oxfordjournals.aob.a086171
23. Flint-Garcia SA (2013) Genetics and consequences of crop domestication. J Agric Food Chem 61: 8267-8276. https://doi.org/10.1021/jf305511d
24. Franz M, Rodriguez H, Lopes C, Zuberi K, Montojo J, Bader GD, Morris Q (2018) GeneMANIA update 2018. Nucleic Acids Res 46: W60-W64. https://doi.org/10.1093/nar/gky311
25. Garcia-Gonzalez F, Simmons LW, Tomkins JL, Kotiaho JS, Evans JP (2012) Comparing evolvabilities: common errors surrounding the calculation and use of coefficients of additive genetic variation.

Evolution 66: 2341-2349. https://doi.org/10.1111/j.1558-5646.2011.01565.x

26. Gaur R, Jeena G, Shah N, Gupta S, Pradhan S, Tyagi AK, Jain M, Chattopadhyay D, Bhatia S (2015) High density linkage mapping of genomic and transcriptomic SNPs for synteny analysis and anchoring the genome sequence of chickpea. Sci Rep 5: 13387. https://doi.org/10.1038/srep13387
27. Govindarajulu R, Hostetler AN, Xiao Y, Chaluvadi SR, Mauro-Herrera M, Siddoway ML, Whipple C, Bennetzen JL, Devos KM, Doust AN, Hawkins JS (2021) Integration of high-density genetic mapping with transcriptome analysis uncovers numerous agronomic QTL and reveals candidate genes for the control of tillering in sorghum. G3 11: jkab024. https://doi.org/10.1093/g3journal/jkab024
28. Gray WM, Muskett PR, Chuang H-w, Parker JE (2003) Arabidopsis SGT1b is required for SCFTIR1-mediated auxin response. Plant Cell 15: 1310-1319. https://doi.org/10.1105/tpc.010884
29. Haley CS, Knott SA (1992) A simple regression method for mapping quantitative trait loci in line crosses using flanking markers. Heredity 69: 315-324. https://doi.org/10.1038/hdy.1992.131
30. Harlan JR (1975) Crops & man. American Society of Agronomy, Crop Science Society of America, Madison.
31. Hodge A (2009) Root decisions. Plant Cell Environ 32: 628-640. https://doi.org/10.1111/j.1365-3040.2008.01891.x
32. Houle D (1992) Comparing evolvability and variability of quantitative traits. Genetics 130: 195-204. https://doi.org/10.1093/genetics/130.1.195
33. Hyten DL, Song Q, Choi I-Y, Yoon M-S, Specht JE, Matukumalli LK, Nelson RL, Shoemaker RC, Young ND, Cregan PB (2008) High-throughput genotyping with the GoldenGate assay in the complex genome of soybean. Theor Appl Genet 116: 945-952. https://doi.org/10.1007/s00122-008-0726-2
34. Jobbágy EG, Jackson RB (2001) The distribution of soil nutrients with depth: global patterns and the imprint of plants. Biogeochemistry 53: 51-77. https://doi.org/10.1023/A:1010760720215
35. Kearsey MJ, Pooni HS (1996) The genetical analysis of quantitative traits. Chapman & Hall, London.
36. Kruse J, Hänsch R, Mendel RR, Rennenberg H (2010) The role of root nitrate reduction in the systemic control of biomass partitioning between leaves and roots in accordance to the C/N-status of tobacco plants. Plant Soil 332: 387-403. https://doi.org/10.1007/s11104-010-0305-6
37. Kumar AA, Sharma HK, Maruthi RT, Kumari N, Jha BK, Choudhary SB (2022) Jute interspecific hybrids: development, characterization and utilization. In: Zhang L, Khan H, Kole C (eds) The jute genome. Compendium of plant genomes. Springer International Publishing, Cham, pp 81-88. https://doi.org/10.1007/978-3-030-91163-8_6
38. Kumar S, Blaxter ML (2010) Comparing *de novo* assemblers for 454 transcriptome data. BMC Genomics 11: 571. https://doi.org/10.1186/1471-2164-11-571
39. Kundu A, Chakraborty A, Mandal NA, Das D, Karmakar PG, Singh NK, Sarkar D (2015) A restriction-site-associated DNA (RAD) linkage map, comparative genomics and identification of QTL for histological fibre content coincident with those for retted bast fibre yield and its major components in jute (*Corchorus olitorius* L., Malvaceae s. l.). Mol Breed 35: 19. https://doi.org/10.1007/s11032-015-0249-x

40. Kundu A, Sarkar D, Mandal NA, Sinha MK, Mahapatra BS (2012) A secondary phloic (bast) fibre-shy (*bfs*) mutant of dark jute (*Corchorus olitorius* L.) develops lignified fibre cells but is defective in cambial activity. Plant Growth Regul 67: 45-55. https://doi.org/10.1007/s10725-012-9660-z
41. Kundu A, Topdar N, Sarkar D, Sinha MK, Ghosh A, Banerjee S, Das M, Balyan HS, Mahapatra BS, Gupta PK (2013) Origins of white (*Corchorus capsularis* L.) and dark (*C. olitorius* L.) jute: a reevaluation based on nuclear and chloroplast microsatellites. J Plant Biochem Biotechnol 22: 372-381. https://doi.org/10.1007/s13562-012-0165-7
42. Ledo A, Paul KI, Burslem DFRP, Ewel JJ, Barton C, Battaglia M, Brooksbank K, Carter J, Eid TH, England JR, Fitzgerald A, Jonson J, Mencuccini M, Montagu KD, Montero G, Mugasha WA, Pinkard E, Roxburgh S, Ryan CM, Ruiz-Peinado R, Sochacki S, Specht A, Wildy D, Wirth C, Zerihun A, Chave J (2018) Tree size and climatic water deficit control root to shoot ratio in individual trees globally. New Phytol 217: 8-11. https://doi.org/10.1111/nph.14863
43. Li H (2011) A quick method to calculate QTL confidence interval. J Genet 90: 355-360. https://doi.org/10.1007/s12041-011-0077-7
44. Lin X, Xiao Y, Song Y, Gan C, Deng X, Wang P, Liu J, Jiang Z, Peng L, Zhou D, He X, Bian J, Zhu C, Liu B, He H, Xu J (2022) Rice microtubule-associated protein OsMAP65-3.1, but not OsMAP65-3.2, plays a critical role in phragmoplast microtubule organization in cytokinesis. Front Plant Sci 13: 1030247. https://doi.org/10.3389/fpls.2022.1030247
45. Liu X, Li R, Chang X, Jing R (2013) Mapping QTLs for seedling root traits in a doubled haploid wheat population under different water regimes. Euphytica 189: 51-66. https://doi.org/10.1007/s10681-012-0690-4
46. Liu Z, Gao K, Shan S, Gu R, Wang Z, Craft EJ, Mi G, Yuan L, Chen F (2017) Comparative analysis of root traits and the associated QTLs for maize seedlings grown in paper roll, hydroponics and vermiculite culture system. Front Plant Sci 8: 436. https://doi.org/10.3389/fpls.2017.00436
47. Løes A-K, Gahoonia TS (2004) Genetic variation in specific root length in Scandinavian wheat and barley accessions. Euphytica 137: 243-249. https://doi.org/10.1023/B:EUPH.0000041587.02009.2e
48. Lopez G, Ahmadi SH, Amelung W, Athmann M, Ewert F, Gaiser T, Gocke MI, Kautz T, Postma J, Rachmilevitch S, Schaaf G, Schnepf A, Stoschus A, Watt M, Yu P, Seidel SJ (2023) Nutrient deficiency effects on root architecture and root-to-shoot ratio in arable crops. Front Plant Sci 13: 1067498. https://doi.org/10.3389/fpls.2022.1067498
49. Lynch JP (2022) Harnessing root architecture to address global challenges. Plant J 109: 415-431. https://doi.org/10.1111/tpj.15560
50. Marschner P (2011) Mineral nutrition of higher plants, 3rd edn. Academic Press, London.
51. Meshram JH, Palit P (2013) On the role of cell wall lignin in determining the fineness of jute fibre. Acta Physiol Plant 35: 1565-1578. https://doi.org/10.1007/s11738-012-1198-1
52. Mgolozeli S, Tesfamariam EH, Beletse Y (2022) Yield, mineral content and root growth response of jute mallow (*Corchorus olitorius* L.) to planting density and water availability. J Agric Food Res 10: 100384. https://doi.org/10.1016/j.jafr.2022.100384

53. Mir RR, Banerjee S, Das M, Gupta V, Tyagi AK, Sinha MK, Balyan HS, Gupta PK (2009) Development and characterization of large-scale simple sequence repeats in jute. Crop Sci 49: 1687-1694. https://doi.org/10.2135/cropsci2008.10.0599
54. Mir RR, Rustgi S, Sharma S, Singh R, Goyal A, Kumar J, Gaur A, Tyagi AK, Khan H, Sinha MK, Balyan HS, Gupta PK (2008) A preliminary genetic analysis of fibre traits and the use of new genomic SSRs for genetic diversity in jute. Euphytica 161: 413-427. https://doi.org/10.1007/s10681-007-9597-x
55. Moose SP, Mumm RH (2008) Molecular plant breeding as the foundation for 21st century crop improvement. Plant Physiol 147: 969-977. https://doi.org/10.1104/pp.108.118232
56. Moriya Y, Itoh M, Okuda S, Yoshizawa AC, Kanehisa M (2007) KAAS: an automatic genome annotation and pathway reconstruction server. Nucleic Acids Res 35: W182-W185. https://doi.org/10.1093/nar/gkm321
57. Moyers BT, Morrell PL, McKay JK (2018) Genetic costs of domestication and improvement. J Hered 109: 103-116. https://doi.org/10.1093/jhered/esx069
58. Paez-Garcia A, Motes C, Scheible W, Chen R, Blancaflor E, Monteros M (2015) Root traits and phenotyping strategies for plant improvement. Plants (Basel) 4: 334-355. https://doi.org/10.3390/plants4020334
59. Pan Y, Qu S, Bo K, Gao M, Haider KR, Weng Y (2017) QTL mapping of domestication and diversifying selection related traits in round-fruited semi-wild Xishuangbanna cucumber (*Cucumis sativus* L. var. xishuangbannanesis). Theor Appl Genet 130: 1531-1548. https://doi.org/10.1007/s00122-017-2908-2
60. Paterson AH (2002) What has QTL mapping taught us about plant domestication? New Phytol 154: 591-608. https://doi.org/10.1046/j.1469-8137.2002.00420.x
61. Perkins AC, Lynch JP (2021) Increased seminal root number associated with domestication improves nitrogen and phosphorus acquisition in maize seedlings. Ann Bot 128: 453-468. https://doi.org/10.1093/aob/mcab074
62. Pierret A, Gonkhamdee S, Jourdan C, Maeght J-L (2013) IJ_Rhizo: an open-source software to measure scanned images of root samples. Plant Soil 373: 531-539. https://doi.org/10.1007/s11104-013-1795-9
63. R Core Team (2022) R: a language and environment for statistical computing. R Foundation for Statistical Computing, Vienna
64. Rich SM, Christopher J, Richards R, Watt M (2020) Root phenotypes of young wheat plants grown in controlled environments show inconsistent correlation with mature root traits in the field. J Exp Bot 71: 4751-4762. http://doi.org/10.1093/jxb/eraa201
65. Richard C, Christopher J, Chenu K, Borrell A, Christopher M, Hickey L (2018) Selection in early generations to shift allele frequency for seminal root angle in wheat. Plant Genome 11: 170071. https://doi.org/10.3835/plantgenome2017.08.0071
66. Richards RA (2008) Genetic opportunities to improve cereal root systems for dryland agriculture. Plant Prod Sci 11: 12-16. https://doi.org/10.1626/pps.11.12

67. Ross-Ibarra J (2005) Quantitative trait loci and the study of plant domestication. Genetica 123: 197-204. https://doi.org/10.1007/s10709-004-2744-6

68. Russi D, Gutierrez Boem FH, Rubio G (2024) Note on the unparallel vertical distribution of nitrate and sulfate in Mollisols. Soil Sci Soc Am J 88: 942-948. https://doi.org/10.1002/saj2.20670

69. Sarkar D, Kundu A, Das D, Chakraborty A, Mandal NA, Satya P, Karmakar PG, Kar CS, Mitra J, Singh NK (2019) Resolving population structure and genetic differentiation associated with RAD-SNP loci under selection in tossa jute (*Corchorus olitorius* L.). Mol Genet Genom 294: 479-492. https://doi.org/10.1007/s00438-018-1526-2

70. Sarkar D, Mahato AK, Satya P, Kundu A, Singh S, Jayaswal PK, Singh A, Bahadur K, Pattnaik S, Singh N, Chakraborty A, Mandal NA, Das D, Basu T, Sevanthi AM, Saha D, Datta S, Kar CS, Mitra J, Datta K, Karmakar PG, Sharma TR, Mohapatra T, Singh NK (2017) The draft genome of *Corchorus olitorius* cv. JRO-524 (Navin). Genom Data 12: 151-154. https://doi.org/10.1016/j.gdata.2017.05.007

71. Sarkar D, Satya P, Mandal NA, Das D, Karmakar PG, Singh NK (2016) Jute genomics: emerging resources and tools for molecular breeding. In: Ramawat KG, Ahuja MR (eds) Fiber plants- biology, biotechnology and applications. Springer International Publishing AG, Cham, pp 155-200. https://doi.org/10.1007/978-3-319-44570-0_9

72. Satya P, Banerjee R, Biswas C, Karan M, Ghosh S, Ali N (2014) Genetic analysis of population structure using peroxidase gene and phenylalanine ammonia-lyase gene-based DNA markers: a case study in jute (*Corchorus* spp.). Crop Sci 54: 1609-1620. https://doi.org/10.2135/cropsci2013.08.0518

73. Satya P, Maiti R (2013) Bast and leaf fibre crops: kenaf, hemp, jute, agave, etc. In: Singh BP (ed) Biofuel crops: production, physiology and genetics. CABI, Wallingford, pp 292–311. https://doi.org/10.1079/9781845938857.0292

74. Satya P, Sarkar D, Chatterjee A, Pal S, Ray S, Sharma L, Roy S, Bera A, Ghosh S, Mitra J, Kar G, Singh NK (2022a) Biosynthesis and chemopreventive potential of jute (*Corchorus capsularis* and *C. olitorius*) flavonoids and phylogeny of flavonoid biosynthesis pathways. Planta Med Int Open 9: e23-e33. https://doi.org/10.1055/a-1712-7978

75. Satya P, Sarkar D, Kar CS, Saha D, Datta S, Pandey SK, Bera A, Mitra J (2022b) Power of molecular markers and genomics technology in jute breeding. In: Zhang L, Khan H, Kole C (eds) The jute genome. Compendium of plant genomes. Springer International Publishing, Cham, pp 321-342. https://doi.org/10.1007/978-3-030-91163-8_21

76. Scheible W-R, Lauerer M, Schulze E-D, Caboche M, Stitt M (1997) Accumulation of nitrate in the shoot acts as a signal to regulate shoot-root allocation in tobacco. Plant J 11: 671-691. https://doi.org/10.1046/j.1365-313X.1997.11040671.x

77. Schmidt JE, Bowles TM, Gaudin ACM (2016) Using ancient traits to convert soil health into crop yield: impact of selection on maize root and rhizosphere function. Front Plant Sci 7: 373. https://doi.org/10.3389/fpls.2016.00373

78. Schneider CA, Rasband WS, Eliceiri KW (2012) NIH Image to ImageJ: 25 years of image analysis. Nat Methods 9: 671-675. https://doi.org/10.1038/nmeth.2089

79. Shannon P, Markiel A, Ozier O, Baliga NS, Wang JT, Ramage D, Amin N, Schwikowski B, Ideker T (2003) Cytoscape: a software environment for integrated models of biomolecular interaction networks. Genome Res 13: 2498-2504. https://doi.org/10.1101/gr.1239303

80. Singh NK, Sarkar D (2022) Jute genome sequencing: an Indian initiative. In: Zhang L, Khan H, Kole C (eds) The jute genome. Compendium of plant genomes. Springer International Publishing, Cham, pp 145-165. https://doi.org/10.1007/978-3-030-91163-8_10

81. Smertenko AP, Chang H-Y, Wagner V, Kaloriti D, Fenyk S, Sonobe S, Lloyd C, Hauser M-T, Hussey PJ (2004) The Arabidopsis microtubule-associated protein AtMAP65-1: molecular analysis of Its microtubule bundling activity. Plant Cell 16: 2035-2047. https://doi.org/10.1105/tpc.104.023937

82. Spoel SH, Dong X (2024) Salicylic acid in plant immunity and beyond. Plant Cell 36: 1451-1464. https://doi.org/10.1093/plcell/koad329

83. Swaminathan MS, Iyer RD (1961) Skewed recombination in a rare interspecific jute hybrid. Nature 192: 893-894. https://doi.org/10.1038/192893b0

84. Szklarczyk D, Kirsch R, Koutrouli M, Nastou K, Mehryary F, Hachilif R, Gable AL, Fang T, Doncheva Nadezhda T, Pyysalo S, Bork P, Jensen Lars J, von Mering C (2023) The STRING database in 2023: protein–protein association networks and functional enrichment analyses for any sequenced genome of interest. Nucleic Acids Res 51: D638-D646. https://doi.org/10.1093/nar/gkac1000

85. Tao A, Huang L, Wu G, Afshar R, Qi J, Xu J, Fang P, Lin L, Zhang L, Lin P (2017) High-density genetic map construction and QTLs identification for plant height in white jute (*Corchorus capsularis* L.) using specific locus amplified fragment (SLAF) sequencing. BMC Genomics 18: 355. https://doi.org/10.1186/s12864-017-3712-8

86. Terrile MC, París R, Calderón-Villalobos LIA, Iglesias MJ, Lamattina L, Estelle M, Casalongué CA (2012) Nitric oxide influences auxin signaling through S-nitrosylation of the Arabidopsis TRANSPORT INHIBITOR RESPONSE 1 auxin receptor. Plant J 70: 492-500. https://doi.org/10.1111/j.1365-313X.2011.04885.x

87. Topdar N, Kundu A, Sinha MK, Sarkar D, Das M, Banerjee S, Kar CS, Satya P, Balyan HS, Mahapatra BS, Gupta PK (2013) A complete genetic linkage map and QTL analyses for bast fibre quality traits, yield and yield components in jute (*Corchorus olitorius* L.). Cytol Genet 47: 129-137. https://doi.org/10.3103/s0095452713030092

88. Tuberosa R, Sanguineti MC, Landi P, Michela Giuliani M, Salvi S, Conti S (2002) Identification of QTLs for root characteristics in maize grown in hydroponics and analysis of their overlap with QTLs for grain yield in the field at two water regimes. Plant Mol Biol 48: 697-712. https://doi.org/10.1023/A:1014897607670

89. Tumber-Dávila SJ, Schenk HJ, Du E, Jackson RB (2022) Plant sizes and shapes above and belowground and their interactions with climate. New Phytol 235: 1032-1056. https://doi.org/10.1111/nph.18031

90. van der Bom FJT, Williams A, Bell MJ (2020) Root architecture for improved resource capture: trade-offs in complex environments. J Exp Bot 71: 5752-5763. https://doi.org/10.1093/jxb/eraa324
91. Van Ooijen JW (2009) MapQTL® 6, software for the mapping of quantitative trait loci in experimental populations of diploid species. Kyazma B. V., Wageningen.
92. Vitor SC, Duarte GT, Saviani EE, Vincentz MGA, Oliveira HC, Salgado I (2013) Nitrate reductase is required for the transcriptional modulation and bactericidal activity of nitric oxide during the defense response of *Arabidopsis thaliana* against Pseudomonas syringae. Planta 238: 475-486. https://doi.org/10.1007/s00425-013-1906-0
93. Voorrips RE (2002) MapChart: software for the graphical presentation of linkage maps and QTLs. J Hered 93: 77-78. https://doi.org/10.1093/jhered/93.1.77
94. Wang B, Liu H, Liu Z, Dong X, Guo J, Li W, Chen J, Gao C, Zhu Y, Zheng X, Chen Z, Chen J, Song W, Hauck A, Lai J (2018) Identification of minor effect QTLs for plant architecture related traits using super high density genotyping and large recombinant inbred population in maize (*Zea mays*). BMC Plant Biol 18: 17. https://doi.org/10.1186/s12870-018-1233-5
95. Wang Z, Huang C, Niu Y, Yung W-S, Xiao Z, Wong F-L, Huang M, Wang X, Man C-K, Sze C-C, Liu A, Wang Q, Chen Y, Liu S, Wu C, Liu L, Hou W, Han T, Li M-W, Lam H-M (2022) QTL analyses of soybean root system architecture revealed genetic relationships with shoot-related traits. Theor Appl Genet 135: 4507-4522. https://doi.org/10.1007/s00122-022-04235-4
96. Wills DM, Burke JM (2007) Quantitative trait locus analysis of the early domestication of sunflower. Genetics 176: 2589-2599. https://doi.org/10.1534/genetics.107.075333
97. Yang Z, Yang Y, Dai Z, Xie D, Tang Q, Cheng C, Xu Y, Liu C, Deng C, Chen J, Su J (2019) Construction of a high-resolution genetic map and identification of quantitative trait loci for salt tolerance in jute (*Corchous* spp.). BMC Plant Biol 19: 391. https://doi.org/10.1186/s12870-019-2004-7
98. Zhao J, Bodner G, Rewald B, Leitner D, Nagel KA, Nakhforoosh A (2017) Root architecture simulation improves the inference from seedling root phenotyping towards mature root systems. J Exp Bot 68: 965-982. http://doi.org/10.1093/jxb/erw494
99. Zhao Y, Wang K, Wang W-l, Yin T-t, Dong W-q, Xu C-j (2019) A high-throughput SNP discovery strategy for RNA-seq data. BMC Genomics 20: 160. https://doi.org/10.1186/s12864-019-5533-4
100. Zhao Y, Zhang H, Xu J, Jiang C, Yin Z, Xiong H, Xie J, Wang X, Zhu X, Li Y, Zhao W, Rashid MAR, Li J, Wang W, Fu B, Ye G, Guo Y, Hu Z, Li Z, Li Z (2018) Loci and natural alleles underlying robust roots and adaptive domestication of upland ecotype rice in aerobic conditions. PLoS Genet 14: e1007521. https://doi.org/10.1371/journal.pgen.1007521
101. Zhou P, Zavaliev R, Xiang Y, Dong X (2023) Seeing is believing: understanding functions of NPR1 and its paralogs in plant immunity through cellular and structural analyses. Curr Opin Plant Biol 73: 102352. https://doi.org/10.1016/j.pbi.2023.102352

Figures

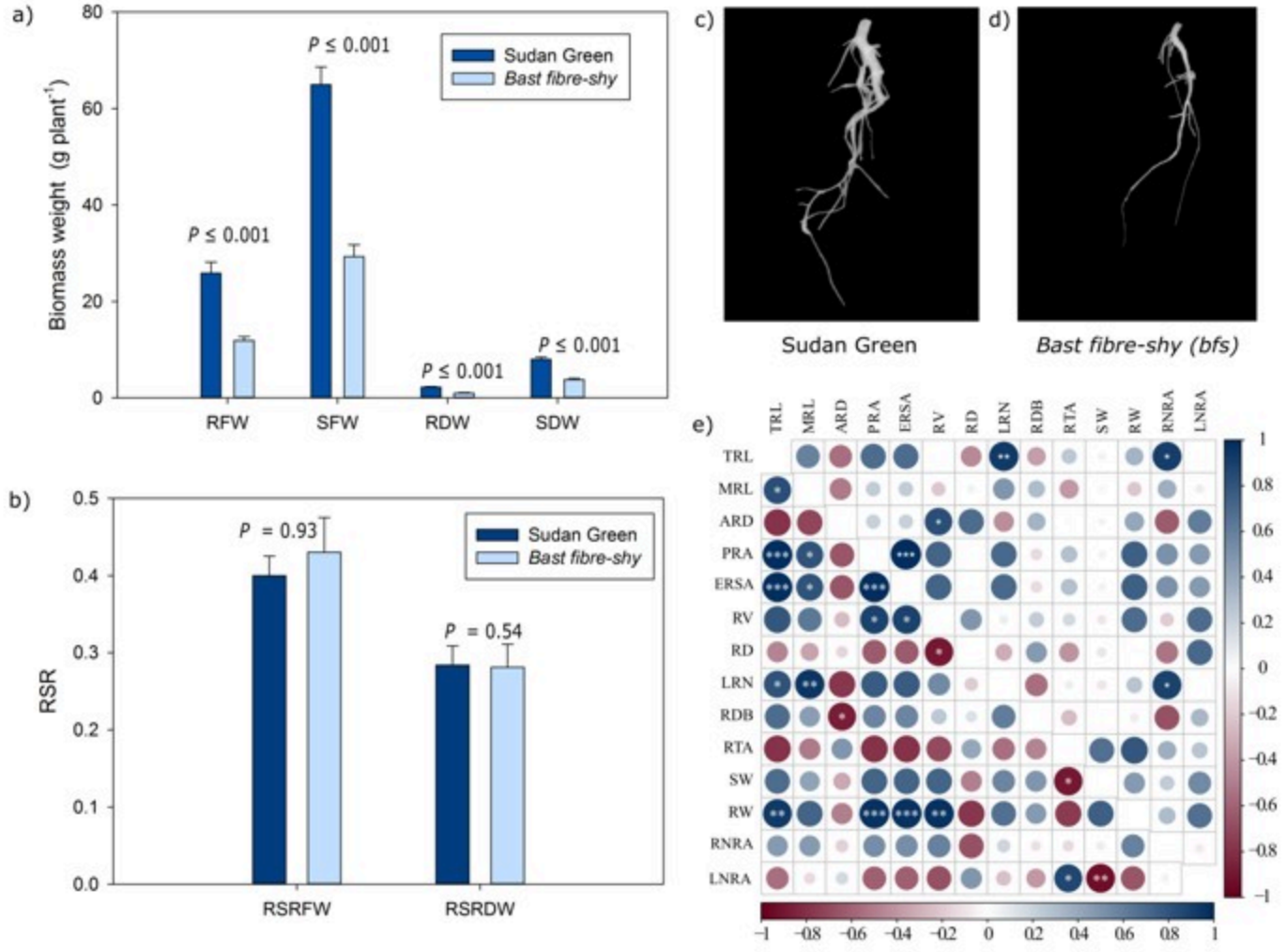

Figure 1

Variations of and associations between the root traits in *C. olitorius* cv. Sudan Green (SG) and its mutant *bfs*, founders of the SG ´ *bfs* mapping population. (**a)** comparative profiles of root versus shoot biomass, (**b)** root to shoot biomass ratios (RSRs) in SG and *bfs*; (**c, d)**SG and *bfs* roots grown under hydroponics for 14 days, **(e)**correlations between the root traits in SG (lower triangle) and *bfs*(upper triangle). Pearson's product-moment correlations are color-coded as per scale. RDW, root dry weight; RFW, root fresh weight; RSRDW, RSR on dry weight basis; RSRFW, RSR on fresh weight basis; SDW, shoot dry weight; SFW, shoot fresh weight. For the other acronyms, see Table 1

Figure 2

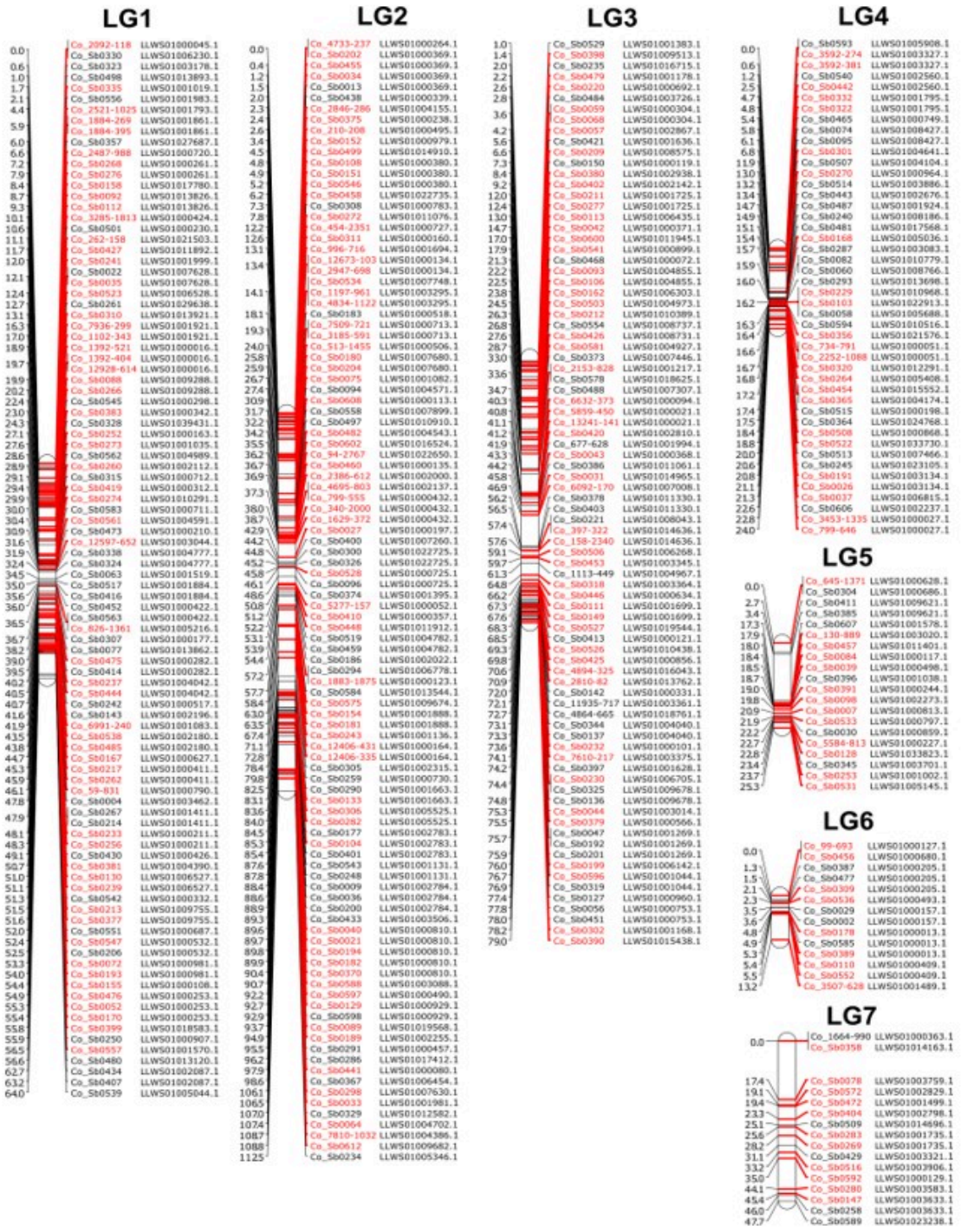

Figure 2

A genome-integrated genetic map of jute (*C. olitorius*) composed of 317 RAD-SNP and 65 genic-SNP loci, with a total genetic length and average marker interval of 365.7 cM and 1.20 cM, respectively across seven linkage groups (LGs). Markers suffixed with alphanumeric and numeric characters represent RAD-SNP and genic-SNP markers, respectively. Gene-associated loci are highlighted in red. RAD, restriction site-associated DNA; SNP, single nucleotide polymorphism

Figure 3

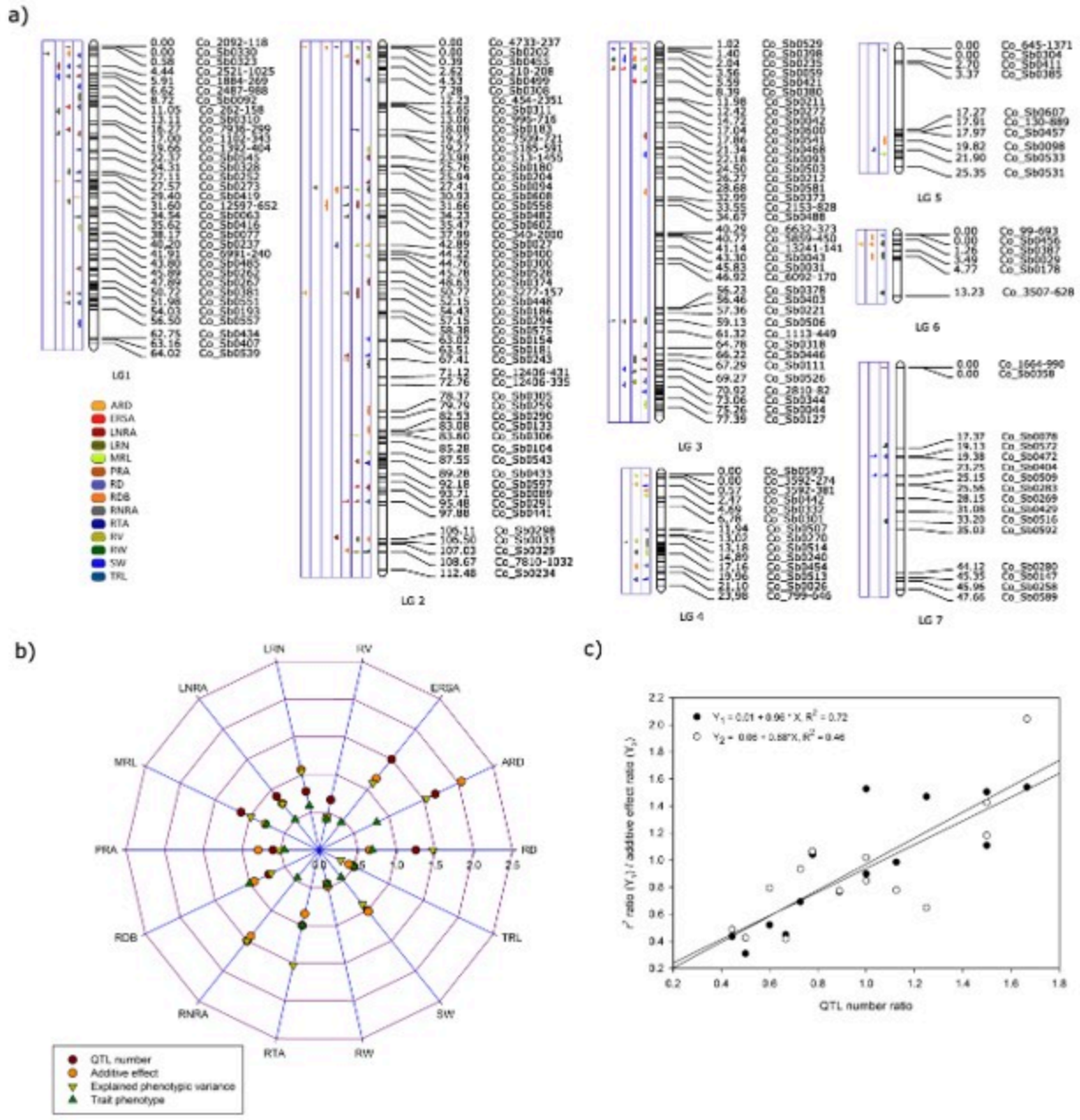

Figure 3

QTL identified for root system architecture, nitrate reductase activities and shoot weight in jute (*C. olitorius*). **(a)** 185 QTL mapped on the *C. olitorius* cv. JRO-524 genome-integrated genetic map. The height of the ovoid-shape represents the width of each QTL, while the center represents the QTL peak position, **(b)**a radar plot of the mutant-WT ratios of the QTL number, additive effect, explained phenotypic variance and trait phenotypes, **(c)** linear regressions of the detected QTL with their additive effects and phenotypic variances. For the other acronyms, see Table 1. WT, wild-type

Figure 4

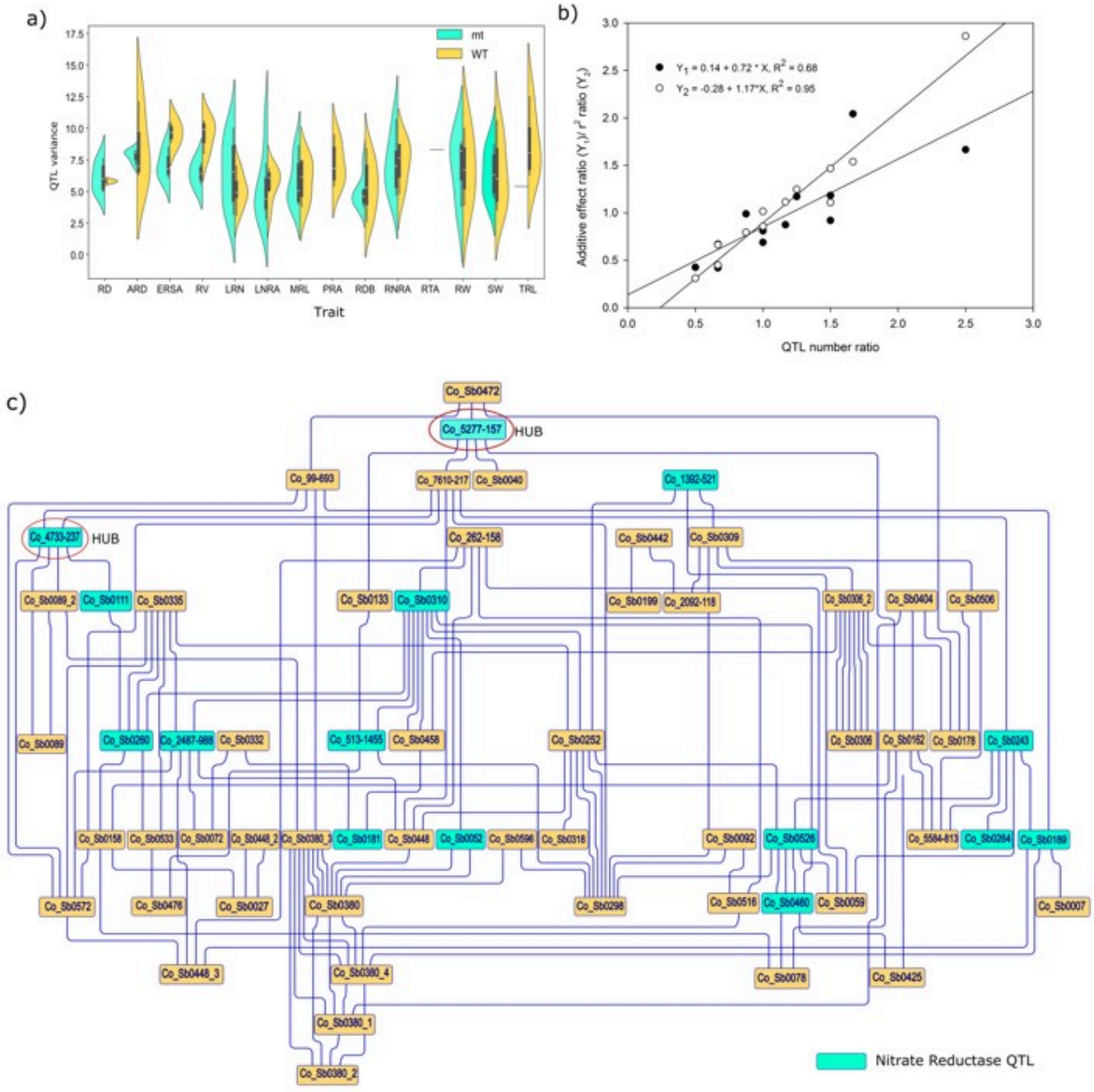

Figure 4

Violin plot and boxplot showing *C. olitorius* cv. Sudan Green (WT) and its corresponding mutant bast-fibre shy (*bfs*) contributing to the variance (r^2) of multi-trait QTL for 14 root traits **(a)**. Linear relationships between the mutant-WT QTL and their phenotypic variance (r^2) ratios for the 48 multi-trait QTL versus all QTL considered **(b)**. Y1 and Y2 denote r^2 ratios of multi-trait and all QTL, respectively. A simplified QTL

gene network for root system architecture showing dependency of the genes associated with the QTL detected, with the nodes corresponding to the genes **(c)**. Values on each node represent the number of genes it is directly linked with. WT, wild-type

Supplementary Files

This is a list of supplementary files associated with this preprint. Click to download.

- satyaetal2025plsoonlineresource1.xlsx